

Electronic Supplementary Information

Design and Synthesis of Chromophores with Enhanced Electro-optic Activities in Both Bulk and Plasmonic-organic Hybrid Devices

Huajun Xu,^a Delwin L. Elder,^{*ab} Lewis E. Johnson,^{*ab} Wolfgang Heni,^{cd} Yovan de Coene,^e Eva De Leo,^{cd} Marcel Destraz,^{cd} Norbert Meier,^c Wouter Vander Ghinst,^e Scott R. Hammond,^{ab} Koen Clays,^e Juerg Leuthold,^{cd} Larry R. Dalton,^a Bruce H. Robinson^a

^a *University of Washington Department of Chemistry, Seattle WA 98195, USA.*

^b *Nonlinear Materials Corporation, Seattle WA 98109, USA.*

^c *Polariton Technologies AG, 8803 Rüslikon, Switzerland.*

^d *Institute of Electromagnetic Fields, ETH Zurich, Gloriastrasse 35, Zurich 8092, Switzerland.*

^e *Department of Chemistry, University of Leuven, Celestijnenlaan 200D, 3001 Leuven, Belgium.*

1 Experimental

1.1 Materials and instrumentation

All chemicals that are commercially available were purchased from Sigma-Aldrich, Acros, Alfa Aesar, or TCI and are used without further purification unless otherwise stated. Tetrahydrofuran (THF), dichloromethane, and toluene solvents were dried by passage through commercial solvent purification system columns (Glass Contour or Pure Process Technology). *N, N*-dimethylformamide (DMF) was purchased in anhydrous form and stored over molecular sieves (pore size 3 Å). 1,1,2-Trichloroethane (TCE) was dried over CaCl₂ for several days then collected via vacuum distillation prior to use. ITO/glass and WRTCO/glass slides were purchased from Thin Film Devices, Inc. TLC analyses were carried out on 0.25 mm thick precoated silica plates and spots were visualized under UV light. Chromatographic purification was carried out on technical grade silica gel (230-400 mesh). ¹H and ¹³C NMR spectra were determined on an Avance Bruker (500 MHz) NMR spectrometer (tetramethylsilane as internal reference). Gas chromatography with mass spectrometry detection (GC/MS) was carried out on an Agilent 7980A or a Hewlett-Packard 6890 gas chromatograph with a quadrupole mass detector. Electrospray ionization mass spectrometry (ESI-MS) was carried out on a Bruker Esquire ion trap mass spectrometer. High-Resolution Mass Spectrometry (HRMS) was performed using a Waters Micromass Quattro Premier XW instrument using electrospray ionization. The UV-Vis spectra were performed on Cary 5000 spectrophotometer. Optical constants (*n* and *k*) were measured by variable angle spectroscopic ellipsometry (VASE) analysis of chromophore thin films on glass substrates using a J. A. Woollam M-2000 instrument. Data were acquired at 55°, 65° and 75°; and fitting was done using Woollam CompleteEASE software. The decomposition temperature (*T_d*) was determined by TGA analysis, performed on a TA5000-2950TGA (TA Instruments) with a heating rate of 10 °C min⁻¹ under the protection of nitrogen. Glass transition temperature (*T_g*) was measured by differential scanning calorimetry (DSC), performed on TA Discovery DSC 2500 with a heating rate of 10 °C min⁻¹ under the protection of nitrogen. Compound **1b** and **2b** were prepared according to the literature method.¹

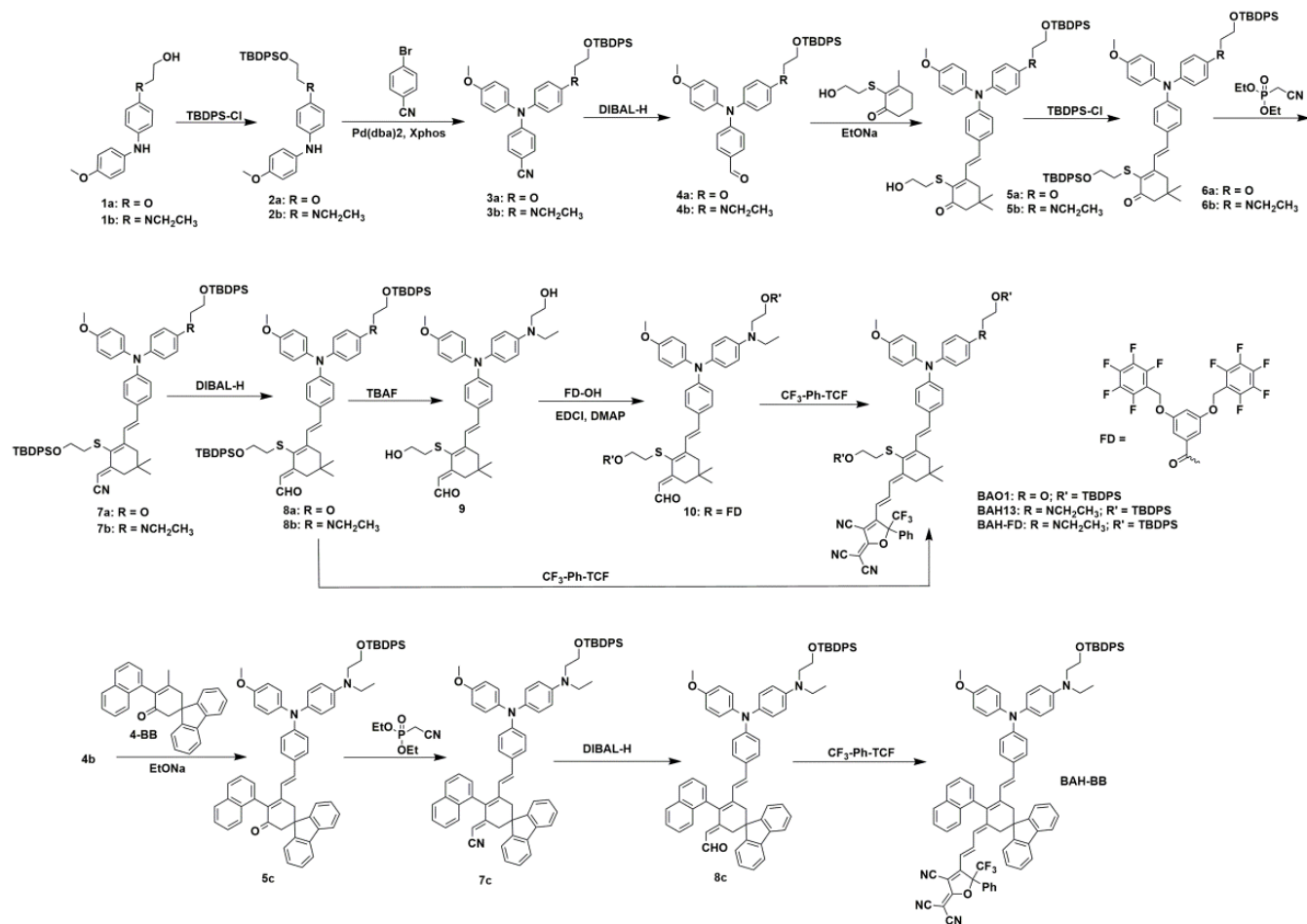


Figure S1. Synthesis route of chromophores.

1.2 Synthesis

Synthesis of 2-{4-[(4-methoxyphenoxy)amino]phenoxy}ethan-1-ol (compound 1a)

In a three-neck round bottom flask, 2-(4-bromophenoxy)ethan-1-ol (25.4 g, 177.0 mmol), 4-methoxyaniline (17.3 g, 140.5 mmol), CuI (0.23 g, 0.01 equiv), diamide ligand (0.28 g, 0.01 equiv) and K_3PO_4 (49.66 g, 2.0 equiv) were placed and evacuated and backfilled with nitrogen. The process was repeated for three times. After that, 150 mL EtOH was added. The reaction mixture was then placed in an oil bath maintaining temperature 80 °C and heating was continued for 24 h. The reaction mixture was then diluted with dichloromethane and filtered through Celite pad and washed it two times with dichloromethane. The product was identified by MS and moved to the next reaction without further purification. MS (ESI) (M^+ , $C_{15}H_{17}NO_3$) calcd: 259.12; found: 259.20.

1.2.2 Synthesis of 4-{2-[(tert-butyldiphenylsilyl)oxy]ethoxy}-N-(4-methoxyphenoxy)aniline (Compound 2a)

In a 50 mL round bottom flask were combined **1** (36 g, 138.8 mmol), imidazole (14 g, 1.5 equiv), and dry DMF (100 mL). After solids dissolved TBDPS-Cl (38.3 g, 139.3 mmol) was added. The solution was stirred for 12 h at room temperature. 200 mL water was added to the solution. The mixture was then extracted by 3 x 50 mL ethyl acetate. The organic layers were combined, washed with brine, dried over $MgSO_4$. Solvent was removed under reduced pressure. Flash chromatography of the crude (acetone: hexane = 1:10 to 1:5) over SiO_2 gave a pale yellow oil in 83% yield. MS (ESI) (M^+ , $C_{31}H_{35}NO_3Si$): calcd: 497.24; found: 497.31. 1H NMR (500 MHz, $CDCl_3$) δ 7.71 (d, J = 6.8 Hz, 4H), 7.38 (m, 6H), 6.93 – 6.85 (m, 4H), 6.78 (t, J = 8.6 Hz, 4H), 4.02 (d, J = 4.7 Hz, 2H), 3.97 (t, J = 4.7 Hz, 2H), 3.73 (s, 3H), 1.07 (s, 9H). ^{13}C NMR (126 MHz, $CDCl_3$) δ 138.12, 135.77, 133.74, 129.79, 127.80, 119.60, 115.75, 114.84, 69.74, 62.91, 55.71, 26.95, 19.36.

Synthesis of 4-[(4-{2-[(tert-butyl)diphenylsilyl]oxy}ethoxy)phenyl](4-methoxyphenyl)amino]benzonitrile (Compound 3a)

In a 500 mL round bottom flask were combined **2a** (19.0 g, 38.2 mmol), 4-Bromobenzonitrile (8.34 g, 1.2 equiv), (0.70 g, 0.02 equiv) tris(dibenzylideneacetone)dipalladium, (0.73 g, 0.04 equiv) XPhos, and (7.34 g, 2.0 mmol) Sodium tert-butoxide and backfilled with nitrogen. To this was added 120 mL dry, degassed toluene, and the reaction was heated to reflux for 24 hr. The reaction mixture was then diluted with dichloromethane and filtered through Celite pad and washed it two times with dichloromethane. The filtrate was dried by roto-evaporator and vacuum oven to give a dark solid without further purification for the next use. Flash chromatography of the crude (acetone: hexane = 1:10 to 1:5) over SiO₂ gave a colorless solid in 87% yield. MS (ESI) (M⁺, C₃₈H₃₈N₂O₃Si): calcd: 598.26; found: 598.15. ¹H NMR (500 MHz, CDCl₃) δ 7.73 (d, *J* = 7.4 Hz, 4H), 7.35 (m, 6H), 7.28 (d, *J* = 8.6 Hz, 2H), 7.06 (t, *J* = 8.7 Hz, 4H), 6.85 (d, *J* = 8.8 Hz, 4H), 6.76 (d, *J* = 8.6 Hz, 2H), 4.06 (t, *J* = 4.7 Hz, 2H), 3.99 (t, *J* = 4.7 Hz, 2H), 3.72 (s, 3H), 1.07 (s, 9H). ¹³C NMR (126 MHz, CDCl₃) δ 157.60, 156.96, 152.43, 138.82, 135.77, 133.69, 133.21, 129.90, 128.11, 127.90, 120.04, 117.29, 116.12, 115.38, 69.58, 62.96, 55.57, 27.05, 19.39.

Synthesis of 4-[4-({2-[(tert-butyl)diphenylsilyl]oxy}ethyl)(ethylamino)phenyl](4-methoxyphenyl)amino} benzonitrile (Compound 3b)

The procedure for compound **3a** was followed to prepare **3b**. The product was moved to the next reaction without further purification. MS (ESI) (M⁺, C₄₀H₄₃N₃O₂Si): calcd: 625.31; found: 625.50.

Synthesis of 4-[(4-{2-[(tert-butyl)diphenylsilyl]oxy}ethoxy)phenyl](4-methoxyphenyl)amino]benzaldehyde (Compound 4a)

In a 100 mL round bottom flask were added **3a** (10.23 g, 17.1 mmol), and backfilled with nitrogen. To this was added 50 mL dry, degassed toluene. After dissolved and cooled to -78 °C, to the solution was added 16 mL diisobutylaluminum hydride (1.2 M in toluene) dropwise. The solution was stirred at -78°C under nitrogen for 2 hours, then the cold bath was removed and the solution stirred a further 2 hours. To hydrolyze, wet silica gel was added, and the solution stirred for 2 hours. To this solution was added MgSO₄. The solution was filtered to remove the silica gel and MgSO₄, and stripped of solvent by rotary evaporator. Flash chromatography of the crude (acetone: hexane = 1:8 to 1:6) over SiO₂ gave a pale yellow solid in 81.1% yield. MS (ESI) (M⁺, C₃₈H₃₉NO₄Si): calcd: 601.26; found: 601.30. ¹H NMR (500 MHz, CDCl₃) δ 9.67 (s, 1H), 7.74 (d, *J* = 6.7 Hz, 4H), 7.57 (d, *J* = 8.0 Hz, 2H), 7.34 (d, *J* = 6.4 Hz, 6H), 7.08 (t, *J* = 7.1 Hz, 4H), 6.84 (d, *J* = 8.4 Hz, 6H), 4.05 (d, *J* = 3.3 Hz, 2H), 4.00 (s, 2H), 3.69 (s, 3H), 1.09 (s, 9H). ¹³C NMR (126 MHz, CDCl₃) δ 189.90, 157.50, 156.87, 154.07, 139.02, 135.70, 133.66, 131.40, 129.84, 128.11, 127.85, 116.98, 116.02, 115.27, 69.51, 62.92, 55.44, 27.01, 19.33.

Synthesis of 4-[4-({2-[(tert-butyl)diphenylsilyl]oxy}ethyl)(ethylamino)phenyl](4-methoxyphenyl)amino} benzaldehyde (Compound 4b)

The procedure for compound **4a** was followed to prepare **4b**. Flash chromatography of the crude (acetone: hexane = 1:8 to 1:6) over SiO₂ gave a yellow solid in 65% yield. MS (ESI) (M⁺, C₄₀H₄₄N₂O₃Si): calcd: 628.31; found: 628.40. ¹H NMR (500 MHz, CDCl₃) δ 9.72 (s, 1H), 7.66 (d, *J* = 7.7 Hz, 4H), 7.59 (d, *J* = 8.6 Hz, 2H), 7.40 (t, *J* = 7.3 Hz, 2H), 7.34 (t, *J* = 7.4 Hz, 4H), 7.13 (d, *J* = 8.7 Hz, 2H), 6.95 (d, *J* = 8.7 Hz, 2H), 6.87 (d, *J* = 8.7 Hz, 2H), 6.80 (d, *J* = 8.5 Hz, 2H), 6.50 (d, *J* = 8.8 Hz, 2H), 3.81 – 3.76 (m, 5H), 3.43 (t, *J* = 6.4 Hz, 2H), 3.33 (q, *J* = 6.9 Hz, 2H), 1.11 (t, *J* = 7.0 Hz, 3H), 1.05 (s, 9H). ¹³C NMR (126 MHz, CDCl₃) δ 190.11, 157.26, 154.52, 146.13, 139.09, 135.66, 133.54, 131.43, 129.77, 128.27, 128.00, 127.77, 116.13, 115.03, 112.51, 61.41, 55.51, 52.12, 45.46, 26.91, 19.15, 12.25.

Synthesis of 3-[(1E)-2-{4-[(4-{2-[(tert-butyl)diphenylsilyl]oxy}ethoxy)phenyl](4-methoxyphenyl)amino}phenyl]

ethenyl]-2-[(2-hydroxyethyl)sulfanyl]-5,5-dimethylcyclohex-2-en-1-one (Compound 5a)

In a 25 mL round bottom flask were added compound **4a** (5.0 g, 9.0 mmol), S-isophorone (2.2 g, 1.2 equiv), and 4 mL THF, then ultrasonic for 5 min. To this was added 12 mL 2M EtONa/EtOH fresh solution. The reaction mixture was heated in microwave oven (50 W/150 °C) for 10 min. After cooling to room temperature, adding a few drops of water quenched the reaction, and all the solvent was removed under reduced pressure by roto-evaporator. The product was moved to the next reaction without further purification. MS (ESI) (M^+ , $C_{49}H_{55}NO_5SSi$): calcd: 797.36; found: 797.10.

Synthesis of 3-[(1E)-2-(4-{4-[(2-[(tert-butylidiphenylsilyl)oxy]ethyl})(ethyl)amino)phenyl](4-methoxyphenyl)amino}phenyl)ethenyl]-2-[(2-hydroxyethyl)sulfanyl]-5,5-dimethylcyclohex-2-en-1-one (Compound 5b)

The procedure for compound **5a** was followed to prepare **5b**. The product was moved to the next reaction without further purification. MS (ESI) (M^+ , $C_{51}H_{60}N_2O_4SSi$): calcd: 824.40; found: 824.30.

Synthesis of 3-[(1E)-2-(4-{4-[(2-[(tert-butylidiphenylsilyl)oxy]ethyl})(ethyl)amino)phenyl](4-methoxyphenyl)amino}phenyl)ethenyl]-4-(naphthalen-1-yl)spiro[cyclohexane-1,9'-fluoren]-3-en-5-one (Compound 5c)

The procedure for compound **5a** was followed to prepare **5c** (yield: 42.4%). MS (ESI) (M^+ , $C_{69}H_{64}N_2O_3Si$): calcd: 996.47; found: 996.40. 1H NMR (500 MHz, $CDCl_3$) δ 7.92 – 7.88 (m, 2H), 7.79 (dd, $J = 11.2, 4.3$ Hz, 2H), 7.75 (d, $J = 7.6$ Hz, 1H), 7.74 (s, 1H), 7.73 – 7.71 (m, 1H), 7.64 (d, $J = 1.4$ Hz, 2H), 7.62 (d, $J = 1.5$ Hz, 2H), 7.59 (dd, $J = 8.2, 7.0$ Hz, 1H), 7.50 – 7.43 (m, 4H), 7.42 (dd, $J = 3.3, 1.6$ Hz, 1H), 7.41 – 7.39 (m, 1H), 7.38 (dd, $J = 3.5, 2.5$ Hz, 1H), 7.37 – 7.35 (m, 1H), 7.35 (s, 1H), 7.33 (s, 1H), 7.31 (s, 2H), 7.30 (dd, $J = 2.4, 1.4$ Hz, 1H), 6.96 (d, $J = 8.9$ Hz, 2H), 6.82 – 6.72 (m, 7H), 6.54 (t, $J = 11.8$ Hz, 3H), 6.39 (d, $J = 8.8$ Hz, 2H), 3.74 (d, $J = 6.5$ Hz, 2H), 3.73 (s, 3H), 3.47 (d, $J = 17.7$ Hz, 1H), 3.37 (t, $J = 6.3$ Hz, 2H), 3.34 (d, $J = 16.1$ Hz, 1H), 3.27 (q, $J = 6.7$ Hz, 2H), 3.12 (d, $J = 17.6$ Hz, 1H), 2.78 (d, $J = 16.8$ Hz, 1H), 1.05 (t, $J = 7.0$ Hz, 3H), 1.03 (s, 9H). ^{13}C NMR (126 MHz, $CDCl_3$) δ 196.60, 150.41, 150.28, 139.62, 139.55, 136.26, 135.57, 135.14, 134.73, 133.76, 133.65, 133.44, 132.69, 129.66, 128.54, 128.33, 128.24, 128.08, 127.74, 127.67, 126.92, 126.10, 125.76, 125.33, 123.83, 123.19, 120.25, 117.84, 114.59, 112.25, 61.27, 55.42, 50.44, 46.85, 45.35, 36.48, 26.81, 19.06.

Synthesis of 3-[(1E)-2-{4-[(4-{2-[(tert-butylidiphenylsilyl)oxy]ethoxy}phenyl)(4-methoxyphenyl)amino]phenyl}ethenyl]-2-[(2-[(tert-butylidiphenylsilyl)oxy]ethyl)sulfanyl]-5,5-dimethylcyclohex-2-en-1-one (Compound 6a)

In a 50 mL round bottom flask were combined **5a** (12.0 g, 15.0 mmol), imidazole (2.1 g, 2.0 equiv), and dry DMF (50 mL). After solids dissolved TBDPS-Cl (6.2 g, 1.5 equiv) was added. The solution was stirred for 12 h at room temperature. 200 mL water was added to the solution. The mixture was then extracted by 3 x 50 mL ethyl acetate. The organic layers were combined, then washed with brine, dried over $MgSO_4$. Solvent was removed under reduced pressure. Flash chromatography of the crude (ethyl acetate: hexane = 1:10) over SiO_2 gave a red solid in 82.0% yields. MS (ESI) (M^+ , $C_{65}H_{73}NO_5SSi_2$): calcd: 1035.47; found: 1035.30. 1H NMR (500 MHz, $CDCl_3$) δ 7.99 (d, $J = 16.1$ Hz, 1H), 7.75 – 7.70 (m, 4H), 7.65 (m, 4H), 7.32 (m, 14H), 7.05 (t, $J = 8.9$ Hz, 2H), 6.99 – 6.96 (m, 1H), 6.94 (d, $J = 8.9$ Hz, 2H), 6.83 (dd, $J = 8.8, 6.4$ Hz, 4H), 6.77 (d, $J = 9.0$ Hz, 2H), 4.05 (m, 2H), 4.01 – 3.96 (m, 2H), 3.77 (t, $J = 6.7$ Hz, 2H), 3.70 (s, 3H), 2.99 (t, $J = 6.7$ Hz, 2H), 2.52 (s, 2H), 2.32 (s, 2H), 1.10 – 1.05 (m, 18H), 1.03 (s, 6H). ^{13}C NMR (126 MHz, $CDCl_3$) δ 195.53, 157.08, 156.65, 156.02, 150.00, 140.20, 135.78, 135.65, 133.69, 129.87, 129.75, 128.84, 127.88, 127.83, 127.30, 125.57, 119.52, 115.78, 115.03, 69.54, 63.68, 62.96, 55.55, 52.11, 36.58, 32.33, 28.50, 27.09, 19.39.

Synthesis of 3-[(1E)-2-(4-{4-[(2-[(tert-butylidiphenylsilyl)oxy]ethyl})(ethyl)amino)phenyl](4-methoxyphenyl)amino}phenyl)ethenyl]-2-[(2-[(tert-butylidiphenylsilyl)oxy]ethyl)sulfanyl]-5,5-dimethylcyclohex-2-en-1-one (Compound 6b)

The procedure for compound **6a** was followed to prepare **6b**. Flash chromatography of the crude (ethyl acetate: hexane = 1:8 to 1:5) over SiO_2 gave a red solid in 78.0% yields. MS (ESI) (M^+ , $C_{47}H_{70}N_2O_4SSi_2$): calcd: 814.46; found: 814.30.

¹H NMR (500 MHz, CDCl₃) δ 7.88 (d, *J* = 16.2 Hz, 1H), 7.66 (dd, *J* = 7.9, 1.4 Hz, 4H), 7.60 (dd, *J* = 7.9, 1.4 Hz, 4H), 7.43 – 7.27 (m, 14H), 7.08 (d, *J* = 8.7 Hz, 2H), 6.92 (m, 3H), 6.84 (d, *J* = 8.9 Hz, 2H), 6.78 (d, *J* = 8.5 Hz, 2H), 6.48 (d, *J* = 8.5 Hz, 2H), 3.81 – 3.77 (m, 5H), 3.72 (t, *J* = 6.9 Hz, 2H), 3.43 (s, 2H), 3.33 (d, *J* = 6.6 Hz, 2H), 2.93 (t, *J* = 6.9 Hz, 2H), 2.53 (s, 2H), 2.33 (s, 2H), 1.11 (t, *J* = 7.0 Hz, 3H), 1.05 (s, 9H), 1.01 (s, 6H), 1.00 (s, 9H). ¹³C NMR (126 MHz, CDCl₃) δ 194.89, 164.10, 156.08, 145.16, 139.92, 135.69, 135.40, 134.73, 133.42, 130.33, 129.56, 129.20, 128.56, 127.61, 126.77, 125.29, 118.21, 114.56, 112.32, 63.41, 55.14, 45.27, 35.32, 34.53, 34.30, 32.19, 31.93, 31.40, 28.14, 27.56, 26.77, 26.59, 25.16, 22.49, 19.06.

Synthesis of 2-[(1E)-3-[(1E)-2-{4-[(4-{2-[(tert-butylidiphenylsilyl)oxy]ethoxy}phenyl)(4-methoxyphenyl)amino]phenyl}ethenyl]-2-[(2-[(tert-butylidiphenylsilyl)oxy]ethyl)sulfanyl]-5,5-dimethylcyclohex-2-en-1-ylidene]acetonitrile (Compound 7a)

Under a nitrogen atmosphere, diethyl(cyanomethyl)phosphonate (4.7 mL, 5.1 g, 28.8 mmol) was slowly added to a two-necked flask charged with NaH (0.69 g, 28.8 mmol) in dry 15 mL THF. The solution was stirred for 10 min in ice bath to clear. Compound **6a** (7.43 g, 7.2 mmol) dissolved in THF (10 mL) was added to the mixture then directly heated to 70 °C for 18 h. The reaction was then cooled, quenched with 20 mL water. The resulting mixture is extracted with 3 x 50 mL ethyl acetate. The resulting organic layer was dried using magnesium sulfate and roto-evaporated to dry. Flash chromatography of the crude (ethyl acetate: hexane = 1:8) over SiO₂ gave a red solid in 45% yields. MS (ESI) (M⁺, C₆₇H₇₄N₂O₄SSi₂): calcd: 1058.49; found: 1058.40. ¹H NMR (500 MHz, CDCl₃) δ 7.87 (d, *J* = 16.2 Hz, 1H), 7.74 – 7.70 (m, 4H), 7.61 (dd, *J* = 10.2, 3.5 Hz, 4H), 7.44 – 7.29 (m, 12H), 7.28 (d, *J* = 8.7 Hz, 2H), 7.06 (d, *J* = 8.9 Hz, 2H), 7.04 (d, *J* = 8.9 Hz, 2H), 6.84 (d, *J* = 8.8 Hz, 4H), 6.81 (d, *J* = 1.8 Hz, 3H), 6.78 (t, *J* = 4.6 Hz, 1H), 6.21 (s, 1H), 4.07 (t, *J* = 5.1 Hz, 2H), 4.00 (t, *J* = 5.0 Hz, 2H), 3.79 (s, 3H), 3.71 (t, *J* = 6.7 Hz, 2H), 2.69 (t, *J* = 6.7 Hz, 2H), 2.49 (s, 2H), 2.39 (s, 2H), 1.07 (s, 9H), 1.04 (s, 9H), 0.95 (s, 6H). ¹³C NMR (126 MHz, CDCl₃) δ 158.19, 156.32, 155.72, 149.41, 148.68, 140.15, 135.62, 135.46, 134.20, 133.51, 133.38, 129.66, 127.66, 127.01, 119.55, 115.53, 114.78, 95.21, 69.33, 63.01, 62.72, 55.46, 43.31, 41.54, 37.60, 30.08, 27.96, 26.82, 19.22.

Synthesis of 2-[(1E)-3-[(1E)-2-(4-{4-[(2-[(tert-butylidiphenylsilyl)oxy]ethyl)(ethyl)amino]phenyl}(4-methoxyphenyl)amino}phenyl)ethenyl]-2-[(2-[(tert-butylidiphenylsilyl)oxy]ethyl)sulfanyl]-5,5-dimethylcyclohex-2-en-1-ylidene]acetonitrile (Compound 7b)

The procedure for compound **7a** was followed to prepare **7b**. Flash chromatography of the crude (ethyl acetate: hexane = 1:10 to 1:6) over SiO₂ gave a red solid in 48% yields. MS (ESI) (M⁺, C₆₉H₇₉N₃O₃SSi₂): calcd: 1085.53; found: 1085.40. ¹H NMR (500 MHz, CDCl₃) δ 7.91 (d, *J* = 15.7 Hz, 1H), 7.70 – 7.61 (m, 8H), 7.36 – 7.24 (m, 12H), 7.23 – 7.19 (m, 2H), 7.07 (d, *J* = 8.1 Hz, 2H), 6.94 (d, *J* = 7.9 Hz, 2H), 6.73 (d, *J* = 6.9 Hz, 2H), 6.50 (d, *J* = 7.9 Hz, 2H), 6.45 (d, *J* = 6.7 Hz, 2H), 6.22 (s, 1H), 6.03 (d, *J* = 6.7 Hz, 1H), 3.81 (s, 3H), 3.72 (t, *J* = 6.9 Hz, 2H), 3.65 (d, *J* = 8.4 Hz, 2H), 3.42 (s, 2H), 3.29 (s, 2H), 2.92 (t, *J* = 6.8 Hz, 3H), 2.69 (t, *J* = 6.1 Hz, 2H), 2.46 (s, 2H), 2.35 (s, 2H), 1.07 (s, 9H), 1.06 (s, 9H), 0.90 (s, 3H), 0.88 (s, 3H). ¹³C NMR (126 MHz, CDCl₃) δ 162.93, 158.00, 155.97, 148.68, 145.08, 140.05, 135.33, 133.16, 129.52, 127.57, 114.53, 112.33, 94.85, 63.39, 55.14, 51.53, 47.64, 35.26, 32.23, 29.82, 27.86, 26.76, 24.19, 19.01.

Synthesis of 2-{3-[(1E)-2-(4-{4-[(2-[(tert-butylidiphenylsilyl)oxy]ethyl)(ethyl)amino]phenyl}(4-methoxyphenyl)amino}phenyl)ethenyl]-4-(naphthalen-1-yl)spiro[cyclohexane-1,9'-fluoren]-3-en-5-ylidene}acetonitrile (Compound 7c)

The procedure for compound **7a** was followed to prepare **7c**. Flash chromatography of the crude (ethyl acetate: hexane = 1:10 to 1:6) over SiO₂ gave a red solid in 45% yields. MS (ESI) (M⁺, C₇₁H₆₅N₃O₂Si): calcd: 1019.48; found: 1019.50. ¹H NMR (500 MHz, CDCl₃) δ 7.93 (d, *J* = 8.0 Hz, 2H), 7.82 (t, *J* = 7.8 Hz, 2H), 7.72 (d, *J* = 8.0 Hz, 1H), 7.64 (dt, *J* = 17.3, 8.5 Hz, 8H), 7.56 – 7.47 (m, 4H), 7.44 (dd, *J* = 15.5, 7.5 Hz, 3H), 7.39 (d, *J* = 9.9 Hz, 1H), 7.36 (d, *J* = 6.8 Hz, 2H), 7.32 (t, *J* = 7.3 Hz, 5H), 6.94 (d, *J* = 6.8 Hz, 2H), 6.82 – 6.67 (m, 7H), 6.56 (t, *J* = 14.5 Hz, 3H), 6.36 (d, *J* = 15.9 Hz, 3H),

3.73 (d, $J = 8.6$ Hz, 5H), 3.37 (dd, $J = 26.5, 17.1$ Hz, 4H), 3.27 (s, 2H), 3.07 (d, $J = 15.6$ Hz, 1H), 2.96 (d, $J = 17.8$ Hz, 1H), 1.06 (t, $J = 6.9$ Hz, 3H), 1.02 (s, 9H). ^{13}C NMR (126 MHz, CDCl_3) δ 158.00, 156.27, 150.90, 150.50, 149.83, 145.38, 142.47, 140.31, 140.11, 139.95, 135.81, 135.24, 134.99, 134.12, 133.65, 132.54, 129.93, 128.73, 127.95, 127.36, 126.98, 126.56, 125.75, 124.29, 123.28, 120.48, 118.39, 114.79, 112.54, 61.60, 53.62, 48.75, 32.21, 30.00, 27.12, 22.98, 19.31, 14.45, 12.48.

Synthesis of 2-[(1E)-3-[(1E)-2-{4-[(4-{2-[(tert-butylidiphenylsilyl)oxy]ethoxy}phenyl)(4-methoxyphenyl)amino]phenyl}ethenyl]-2-[(2-[(tert-butylidiphenylsilyl)oxy]ethyl)sulfanyl]-5,5-dimethylcyclohex-2-en-1-ylidene]acetaldehyde (Compound 8a)

In a 100 mL round bottom flask were added **7a** (3.34 g, 3.15 mmol), and backfilled with nitrogen. To this was added 15 mL dry, degassed toluene. After dissolved and cooled to -78 °C, to the solution was added 5.2 mL diisobutylaluminum hydride (1.2 M in toluene) dropwise. The solution became red immediately. The solution was stirred at -78 °C under nitrogen for 2 hours, then the cold bath was removed and the solution stirred a further 1 hours. To hydrolyze, wet silica gel was added, and the solution stirred for 2 hour. To this solution was added MgSO_4 . The solution was filtered to remove the silica gel and MgSO_4 , and stripped of solvent by rotary evaporator. Flash chromatography of the crude (ethyl acetate: hexane = 1:8) over SiO_2 gave an orange solid in 83% yields. MS (ESI) (M^+ , $\text{C}_{67}\text{H}_{75}\text{NO}_5\text{SSi}_2$): calcd: 1061.49; found: 1061.30. ^1H NMR (500 MHz, CDCl_3) δ 10.11 (d, $J = 7.9$ Hz, 1H), 8.00 (d, $J = 16.1$ Hz, 1H), 7.73 (d, $J = 6.4$ Hz, 4H), 7.61 (d, $J = 6.7$ Hz, 4H), 7.41 – 7.26 (m, 13H), 7.08 – 7.02 (m, 4H), 6.99 (d, $J = 7.9$ Hz, 1H), 6.86 – 6.78 (m, 8H), 4.06 (t, $J = 5.0$ Hz, 2H), 4.00 (t, $J = 4.9$ Hz, 2H), 3.77 – 3.72 (m, 5H), 2.73 (t, $J = 6.8$ Hz, 2H), 2.62 (s, 2H), 2.41 (s, 2H), 1.08 (s, 9H), 1.03 (s, 9H), 0.96 (s, 6H). ^{13}C NMR (126 MHz, CDCl_3) δ 191.23, 156.27, 155.90, 155.65, 149.53, 149.31, 140.11, 135.55, 133.94, 133.44, 129.62, 129.27, 128.61, 128.17, 127.62, 127.12, 126.94, 126.49, 119.53, 115.49, 114.73, 69.28, 63.19, 62.69, 55.35, 41.49, 39.68, 37.33, 29.86, 28.20, 26.80, 19.16.

Synthesis of 2-[(1E)-3-[(1E)-2-(4-{4-[(2-[(tert-butylidiphenylsilyl)oxy]ethyl)(ethyl)amino]phenyl}(4-methoxyphenyl)amino)phenyl]ethenyl]-2-[(2-[(tert-butylidiphenylsilyl)oxy]ethyl)sulfanyl]-5,5-dimethylcyclohex-2-en-1-ylidene]acetaldehyde (Compound 8b)

The procedure for compound **8a** was followed to prepare **8b**. Flash chromatography of the crude (ethyl acetate: hexane = 1:8) over SiO_2 gave a red solid in 78% yields. MS (ESI) (M^+ , $\text{C}_{69}\text{H}_{80}\text{N}_2\text{O}_4\text{SSi}_2$): calcd: 1088.54; found: 1088.42. ^1H NMR (500 MHz, CDCl_3) δ 10.10 (d, $J = 7.8$ Hz, 1H), 8.01 (d, $J = 15.8$ Hz, 1H), 7.68 (d, $J = 7.6$ Hz, 4H), 7.62 (d, $J = 7.6$ Hz, 4H), 7.30 (m, 16H), 7.07 (d, $J = 8.6$ Hz, 2H), 7.02 (d, $J = 7.5$ Hz, 1H), 6.94 (d, $J = 8.5$ Hz, 2H), 6.80 (t, $J = 9.0$ Hz, 6H), 6.50 (d, $J = 8.7$ Hz, 2H), 3.81 (t, $J = 5.7$ Hz, 2H), 3.76 (t, $J = 6.7$ Hz, 2H), 3.67 (s, 3H), 3.43 (s, 2H), 3.30 (d, $J = 5.8$ Hz, 2H), 2.74 (t, $J = 6.6$ Hz, 2H), 2.59 (s, 2H), 2.39 (s, 2H), 1.07 (s, 9H), 1.04 (s, 9H), 0.93 (s, 6H). ^{13}C NMR (126 MHz, CDCl_3) δ 190.90, 155.97, 155.76, 149.68, 145.09, 140.08, 135.41, 135.06, 134.19, 133.30, 129.58, 128.73, 128.10, 127.60, 126.88, 126.64, 125.82, 118.44, 114.53, 112.33, 63.16, 61.29, 55.17, 51.98, 45.27, 41.36, 39.57, 37.29, 29.70, 28.10, 26.77, 19.03, 12.17.

Synthesis of 2-{3-[(1E)-2-(4-{4-[(2-[(tert-butylidiphenylsilyl)oxy]ethyl)(ethyl)amino]phenyl}(4-methoxyphenyl)amino)phenyl]ethenyl}-4-(naphthalen-1-yl)spiro[cyclohexane-1,9'-fluoren]-3-en-5-ylidene]acetaldehyde (Compound 8c)

The procedure for compound **8a** was followed to prepare **8c**. Flash chromatography of the crude (ethyl acetate: hexane = 1:8) over SiO_2 gave a red solid in 78% yields. MS (ESI) (M^+ , $\text{C}_{71}\text{H}_{66}\text{N}_2\text{O}_3\text{Si}$): calcd: 1022.48; found: 1022.35. ^1H NMR (500 MHz, CDCl_3) δ 9.73 (d, $J = 8.0$ Hz, 1H), 7.91 (d, $J = 8.0$ Hz, 2H), 7.82 (dd, $J = 10.9, 7.2$ Hz, 2H), 7.74 (d, $J = 8.2$ Hz, 1H), 7.69 (t, $J = 7.5$ Hz, 2H), 7.63 (d, $J = 6.6$ Hz, 4H), 7.61 – 7.57 (m, 1H), 7.52 – 7.43 (m, 4H), 7.42 (d, $J = 7.7$ Hz, 1H), 7.39 (d, $J = 7.6$ Hz, 1H), 7.36 (d, $J = 7.0$ Hz, 2H), 7.34 – 7.27 (m, 5H), 6.94 (d, $J = 8.7$ Hz, 2H), 6.78 (d, $J = 8.6$ Hz, 2H), 6.74 (d, $J = 8.9$ Hz, 2H), 6.71 (d, $J = 8.8$ Hz, 2H), 6.59 (d, $J = 16.2$ Hz, 1H), 6.55 (d, $J = 8.5$ Hz, 2H), 6.40 (t, $J =$

11.9 Hz, 2H), 5.51 (d, $J = 7.8$ Hz, 1H), 3.76 – 3.71 (m, 5H), 3.47 (d, $J = 15.8$ Hz, 1H), 3.42 – 3.33 (m, 4H), 3.27 (q, $J = 7.1$ Hz, 2H), 3.00 (d, $J = 18.0$ Hz, 1H), 1.06 (t, $J = 7.0$ Hz, 3H), 1.03 (s, 9H).

Synthesis of 2-[(1E)-3-[(1E)-2-[4-[(4-ethyl(2-hydroxyethyl)amino]phenyl)(4-methoxyphenyl)amino]phenyl]ethenyl]-2-[(2-hydroxyethyl)sulfanyl]-5,5-dimethylcyclohex-2-en-1-ylidene]acetaldehyde (Compound 9)

A round bottom flask was charged with compound **8b** (1.09 g, 1.0 mmol), purged with nitrogen, and dissolved in 10 mL THF. To this was added tetrabutylammonium fluoride solution (1.0 M in THF, 3.0 mL) in dropwise. After 1 hour, the solution was worked up by stripping off the solvent, then adding 50 mL of NH_4Cl /water. Then the aqueous layer was extracted with 3 x 50 mL ethyl acetate, the combined organic layers were dried over MgSO_4 , filtered, and stripped of solvent by rotary evaporation. The crude product was used for the next step without further purification. MS (ESI) (M^+ , $\text{C}_{37}\text{H}_{44}\text{N}_2\text{O}_4\text{S}$): calcd: 612.30; found: 612.30. ^1H NMR (500 MHz, CDCl_3) δ 10.10 (t, $J = 10.0$ Hz, 1H), 7.96 (d, $J = 15.2$ Hz, 1H), 7.32 (s, 2H), 7.08 (s, 2H), 7.00 (d, $J = 7.8$ Hz, 3H), 6.83 (d, $J = 7.7$ Hz, 5H), 6.70 (s, 2H), 3.77 (d, $J = 11.8$ Hz, 5H), 3.65 – 3.59 (m, 2H), 3.40 (s, 2H), 2.74 (s, 4H), 2.50 (s, 2H), 2.28 (s, 2H), 1.15 (t, $J = 6.9$ Hz, 3H), 1.03 (s, 6H). ^{13}C NMR (126 MHz, CDCl_3) δ 191.66, 156.67, 126.89, 114.72, 61.21, 55.48, 41.69, 39.88, 38.12, 31.56, 30.07, 28.27, 25.27, 22.63, 14.11.

Synthesis of 2-[(6E)-2-[(1E)-2-[4-[(2-{3,5-bis[(2,3,4,5,6-pentafluorophenyl)methoxy]benzoyloxy}ethyl)(ethyl)amino]phenyl](4-methoxyphenyl)amino]phenyl]ethenyl]-4,4-dimethyl-6-(2-oxoethylidene)cyclohex-1-en-1-yl]sulfanyl]ethyl 3,5-bis[(2,3,4,5,6-pentafluorophenyl)methoxy]benzoate (Compound 10)

Under a nitrogen atmosphere, N,N -dimethylaminopyridine (0.015g, 0.12 mmol), EDCI (0.24 g, 1.2 mmol), FD-OH (0.62 g, 1.2 mmol) in 5 mL dichloromethane was cooled to 0 °C. After the solution became clear, compound 9 (0.31 g, 0.5 mmol) in 2 mL dichloromethane were added. The mixture was stirred for overnight at room temperature after at 0 °C for 2h. The crude product was then purified by silica gel chromatography eluting with ethyl acetate/hexane (1:5 to 1:3) to afford a red solid **10** in 78% yields. MS (ESI) (M^+ , $\text{C}_{79}\text{H}_{56}\text{F}_{20}\text{N}_2\text{O}_{10}\text{S}$): calcd: 1604.33; found: 1604.30. ^1H NMR (500 MHz, CDCl_3) δ 10.15 (d, $J = 7.8$ Hz, 1H), 7.93 (d, $J = 15.4$ Hz, 1H), 7.33 (d, $J = 5.8$ Hz, 2H), 7.27 (s, 1H), 7.20 (s, 2H), 7.02 (d, $J = 25.6$ Hz, 5H), 6.85 – 6.75 (m, 5H), 6.69 (d, $J = 15.9$ Hz, 5H), 5.10 (s, 4H), 5.04 (s, 4H), 4.47 (d, $J = 5.3$ Hz, 2H), 4.39 – 4.35 (m, 2H), 3.78 (s, 3H), 3.67 (s, 2H), 3.44 (s, 2H), 2.96 – 2.90 (m, 2H), 2.73 (s, 2H), 2.45 (s, 2H), 1.02 (s, 6H).

Synthesis of 2-[4-[(1E)-3-[(1E)-3-[(1E)-2-[4-[(4-{2-[(tert-butyl)diphenylsilyl]oxy}ethoxy]phenyl)(4-methoxyphenyl)amino]phenyl]ethenyl]-2-[(2-[(tert-butyl)diphenylsilyl]oxy)ethyl]sulfanyl)-5,5-dimethylcyclohex-2-en-1-ylidene]prop-1-en-1-yl]-3-cyano-5-phenyl-5-(trifluoromethyl)-2,5-dihydrofuran-2-ylidene]propanedinitrile (BAO1)

Compound **8a** (0.36 g, 0.29 mmol) and acceptor CF_3PhTCF (0.11 g, 1.2 equiv) were dissolved by benzene (1.5 mL), then anhydrous ethanol (1.5 mL) was added. The mixture was allowed to stir at 60 °C for 1h with TLC trace. The solvent was removed under vacuum and the residual mixture was purified by flash chromatography on silica gel (hexane/acetone (10:1 to 8:1) to afford chromophore **BAO1** as a dark solid in 82 % yield. HRMS (ESI) (M^+ , $\text{C}_{83}\text{H}_{81}\text{F}_3\text{N}_4\text{O}_5\text{SSi}_2$): calcd: 1358.5418; found: 1358.5420. ^1H NMR (500 MHz, CDCl_3) δ 8.04 (d, $J = 13.2$ Hz, 1H), 7.99 (d, $J = 15.9$ Hz, 1H), 7.71 (d, $J = 7.9$ Hz, 4H), 7.57 (d, $J = 6.8$ Hz, 4H), 7.50 (m, 5H), 7.45 – 7.40 (m, 3H), 7.40 – 7.33 (m, 6H), 7.32 – 7.24 (m, 6H), 7.07 (d, $J = 8.8$ Hz, 2H), 7.04 (d, $J = 8.8$ Hz, 2H), 6.92 (d, $J = 16.0$ Hz, 1H), 6.86 (d, $J = 8.9$ Hz, 2H), 6.83 (d, $J = 8.9$ Hz, 2H), 6.79 (d, $J = 8.6$ Hz, 2H), 6.44 (d, $J = 14.6$ Hz, 1H), 4.08 (t, $J = 4.9$ Hz, 2H), 4.00 (t, $J = 5.0$ Hz, 2H), 3.81 (s, 3H), 3.70 (t, $J = 6.6$ Hz, 2H), 2.69 (t, $J = 6.6$ Hz, 2H), 2.45 (s, 2H), 2.22 (m, 2H), 1.06 (s, 9H), 1.00 (s, 9H), 0.92 (s, 3H), 0.85 (s, 3H). ^{13}C NMR (126 MHz, CDCl_3) δ 175.62, 171.02, 162.92, 157.75, 156.88, 156.25, 153.55, 150.38, 147.45, 139.81, 137.09, 135.74, 135.56, 133.67, 133.52, 131.48, 131.29, 130.06, 129.84, 129.14, 128.78, 128.39, 127.80, 127.44, 126.83,

126.49, 119.21, 117.35, 115.80, 115.04, 111.48, 111.25, 110.77, 69.54, 63.11, 62.89, 60.39, 55.60, 41.84, 41.22, 38.42, 30.41, 28.54, 27.95, 26.96, 21.08, 19.39, 14.32.

Synthesis of 2-{4-[(1E)-3-[(1E)-3-[(1E)-2-(4-{4-{2-[(tert-butylidiphenylsilyl)oxy]ethyl}(ethylamino)phenyl](4-methoxyphenyl)amino}phenyl)ethenyl]-2-[(2-[(tert-butylidiphenylsilyl)oxy]ethyl)sulfanyl]-5,5-dimethylcyclohex-2-en-1-ylidene]prop-1-en-1-yl]-3-cyano-5-phenyl-5-(trifluoromethyl)-2,5-dihydrofuran-2-ylidene}propanedinitrile (BAH13)

The procedure for **BAO1** was followed to prepare **BAH13**. Flash chromatography of the crude (acetone: hexane = 1:8) over SiO₂ gave a dark solid in 69% yields. HRMS (ESI) (M⁺, C₈₅H₈₆F₃N₅O₄SSi₂): calcd: 1385.5891; found: 1385.5880. ¹H NMR (500 MHz, CDCl₃) δ 8.04 (t, *J* = 12.3 Hz, 1H), 7.96 (d, *J* = 16.3 Hz, 1H), 7.66 (d, *J* = 7.1 Hz, 4H), 7.57 (d, *J* = 7.2 Hz, 4H), 7.50 (m, 5H), 7.41 (t, *J* = 11.0 Hz, 3H), 7.35 (t, *J* = 7.5 Hz, 6H), 7.31 – 7.23 (m, 6H), 7.08 (d, *J* = 7.1 Hz, 2H), 6.92 (d, *J* = 16.2 Hz, 3H), 6.84 (d, *J* = 7.9 Hz, 2H), 6.76 (d, *J* = 7.2 Hz, 2H), 6.48 (d, *J* = 6.2 Hz, 2H), 6.42 (d, *J* = 14.7 Hz, 1H), 2.68 (t, *J* = 6.5 Hz, 5H), 2.44 (s, 2H), 2.22 (dd, *J* = 42.4, 14.9 Hz, 2H), 1.11 (t, *J* = 6.8 Hz, 3H), 1.04 (s, 9H), 0.99 (s, 9H), 0.92 (s, 3H), 0.84 (s, 3H). ¹³C NMR (126 MHz, CDCl₃) δ 175.62, 171.10, 162.65, 157.90, 147.29, 135.61, 135.45, 133.46, 133.36, 131.30, 130.01, 129.71, 129.65, 127.71, 127.67, 126.73, 117.02, 114.74, 112.32, 111.55, 111.24, 110.75, 62.98, 60.37, 57.90, 55.50, 41.70, 41.09, 38.20, 30.32, 28.42, 27.87, 26.84, 26.80, 21.03, 19.19, 19.09, 14.20.

Synthesis of 2-[(6E)-2-[(1E)-2-[4-[(2-{3,5-bis[(2,3,4,5,6-pentafluorophenyl)methoxy]benzoyloxy]ethyl}(ethylamino)phenyl](4-methoxyphenyl)amino)phenyl]ethenyl]-6-[(2E)-3-[4-cyano-5-(dicyanomethylidene)-2-phenyl-2-(trifluoromethyl)-2,5-dihydrofuran-3-yl]prop-2-en-1-ylidene]-4,4-dimethylcyclohex-1-en-1-yl]sulfanyl]ethyl 3,5-bis[(2,3,4,5,6-pentafluorophenyl)methoxy]benzoate (BAH-FD)

The procedure for **BAO1** was followed to prepare **BAH-FD**. Flash chromatography of the crude (acetone: hexane = 1:8) over SiO₂ gave a dark solid in 69% yields. HRMS (ESI) (M⁺, C₉₅H₆₂F₂₃N₅O₁₀S): calcd: 1901.3850; found: 1901.3833. ¹H NMR (500 MHz, CDCl₃) δ 7.97 (d, *J* = 15.8 Hz, 1H), 7.55 – 7.47 (m, 5H), 7.40 (d, *J* = 12.3 Hz, 1H), 7.32 (d, *J* = 2.3 Hz, 2H), 7.23 (d, *J* = 2.3 Hz, 3H), 7.21 (s, 1H), 7.06 (d, *J* = 8.0 Hz, 2H), 7.01 (d, *J* = 7.9 Hz, 2H), 6.91 (d, *J* = 15.9 Hz, 1H), 6.82 (d, *J* = 8.7 Hz, 2H), 6.78 (t, *J* = 2.3 Hz, 1H), 6.73 – 6.67 (m, 5H), 6.47 (d, *J* = 14.6 Hz, 1H), 5.10 (s, 4H), 5.02 (s, 4H), 4.47 (t, *J* = 6.3 Hz, 2H), 4.35 (d, *J* = 4.8 Hz, 2H), 3.79 (s, 3H), 3.67 (s, 2H), 3.44 (s, 2H), 2.92 (t, *J* = 6.9 Hz, 2H), 2.47 (d, *J* = 3.9 Hz, 2H), 2.27 (dd, *J* = 42.9, 15.0 Hz, 2H), 1.20 (t, *J* = 7.0 Hz, 3H), 0.96 (s, 3H), 0.87 (s, 3H). ¹³C NMR (126 MHz, CDCl₃) δ 175.55, 165.87, 165.46, 159.29, 146.89, 144.91, 142.18, 140.21, 138.39, 132.27, 132.02, 131.37, 130.05, 129.71, 126.79, 111.20, 110.70, 108.98, 107.83, 107.69, 107.54, 107.17, 70.99, 63.67, 58.04, 55.40, 41.78, 41.15, 30.36, 28.50, 27.74, 15.38.

Synthesis of N¹-{2-[(tert-butylidiphenylsilyl)oxy]ethyl}-N¹-ethyl-N⁴-{4-[(1E)-2-[(5E)-5-[(2E)-3-[4-ethynyl-5-(penta-1,4-diyne-3-ylidene)-2-phenyl-2-(trifluoromethyl)-2,5-dihydrofuran-3-yl]prop-2-en-1-ylidene]-4-(naphthalen-1-yl)spiro[cyclohexane-1,9'-fluoren]-3-en-3-yl]ethenyl]phenyl}-N⁴-(4-methoxyphenyl)benzene-1,4-diamine (BAH-BB)

The procedure for **BAO1** was followed to prepare **BAH-BB**. Flash chromatography of the crude (acetone: hexane = 1:8) over SiO₂ gave a red solid in 41% yields. HRMS (ESI) (M⁺, C₈₇H₇₂F₃N₅O₃Si): calcd: 1319.5356; found: 1319.5333. ¹H NMR (500 MHz, C₆D₆) δ 7.89 (d, *J* = 8.4 Hz, 1H), 7.72 (d, *J* = 8.1 Hz, 1H), 7.68 (m, 7.62 (d, *J* = 7.5 Hz, 1H), 7.59 (d, *J* = 7.6 Hz, 1H), 7.37 – 7.19 (m, 9H), 7.16 (d, *J* = 5.9 Hz, 6H), 7.00 – 6.83 (m, 5H), 6.73 (d, *J* = 8.3 Hz, 2H), 6.66 (d, *J* = 16.9 Hz, 1H), 6.64 – 6.58 (m, 6H), 6.48 – 6.39 (m, 3H), 6.34 (s, 2H), 5.89 (d, *J* = 12.1 Hz, 1H), 5.52 (d, *J* = 14.8 Hz, 1H), 3.64 (t, *J* = 6.0 Hz, 2H), 3.23 (s, 3H), 3.17 (s, 2H), 3.09 (d, *J* = 17.9 Hz, 1H), 2.95 (d, *J* = 15.5 Hz, 3H), 2.79 (d, *J* = 18.1 Hz, 1H), 2.25 (d, *J* = 15.6 Hz, 1H), 1.12 (s, 9H), 0.80 (t, *J* = 6.9 Hz, 3H). ¹³C NMR (126 MHz, CDCl₃) δ 150.67, 150.29, 149.99, 139.65, 135.58, 133.86, 133.44, 131.20, 129.67, 129.33, 129.04, 128.76, 128.28, 128.18, 127.99, 127.77, 127.68,

126.83, 126.50, 126.38, 125.55, 125.46, 123.84, 123.08, 120.27, 120.12, 110.57, 55.43, 48.63, 29.69, 26.81, 19.07.

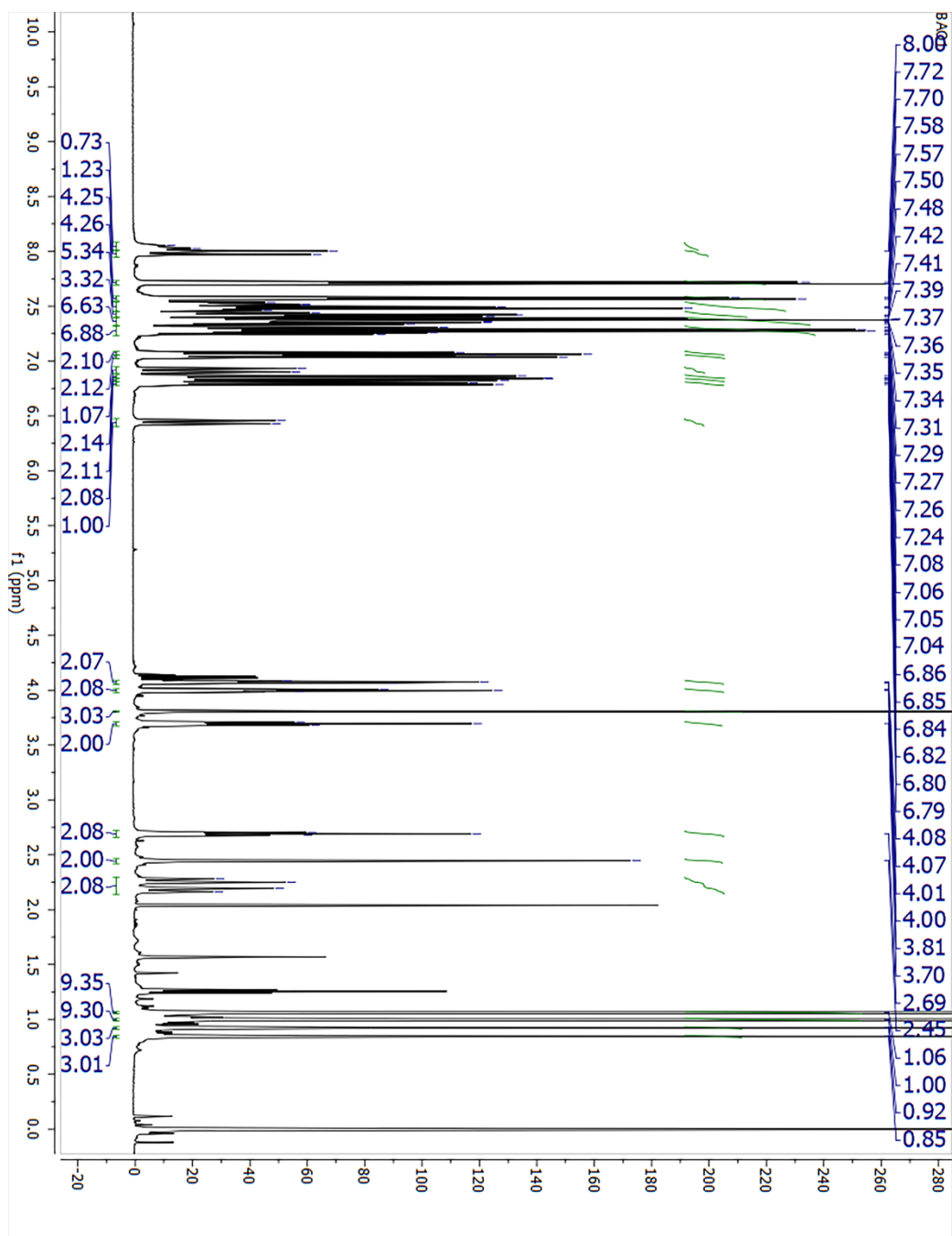


Figure S2. ^1H NMR spectrum of BAO1.

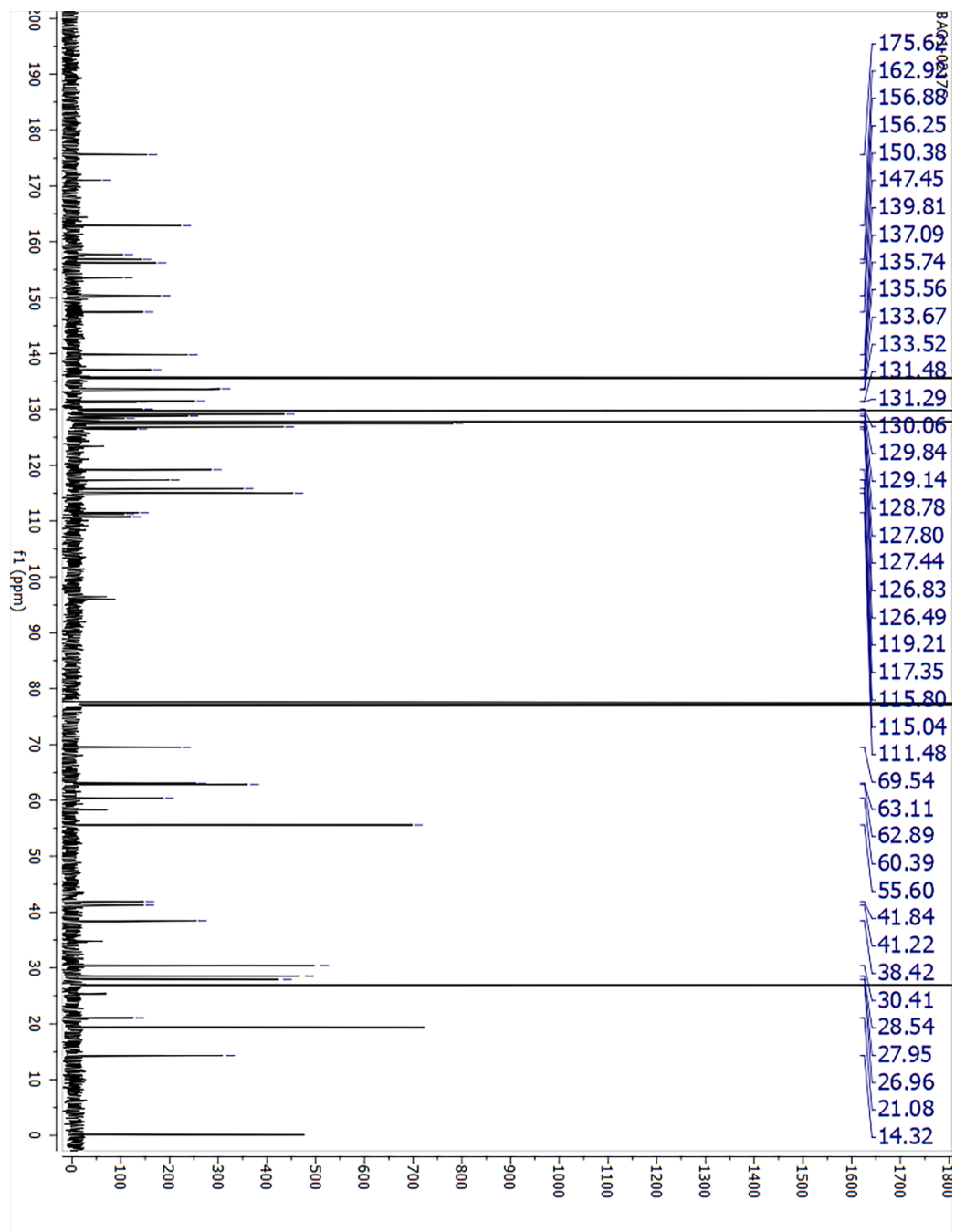


Figure S3. ^{13}C NMR spectrum of BAO1.

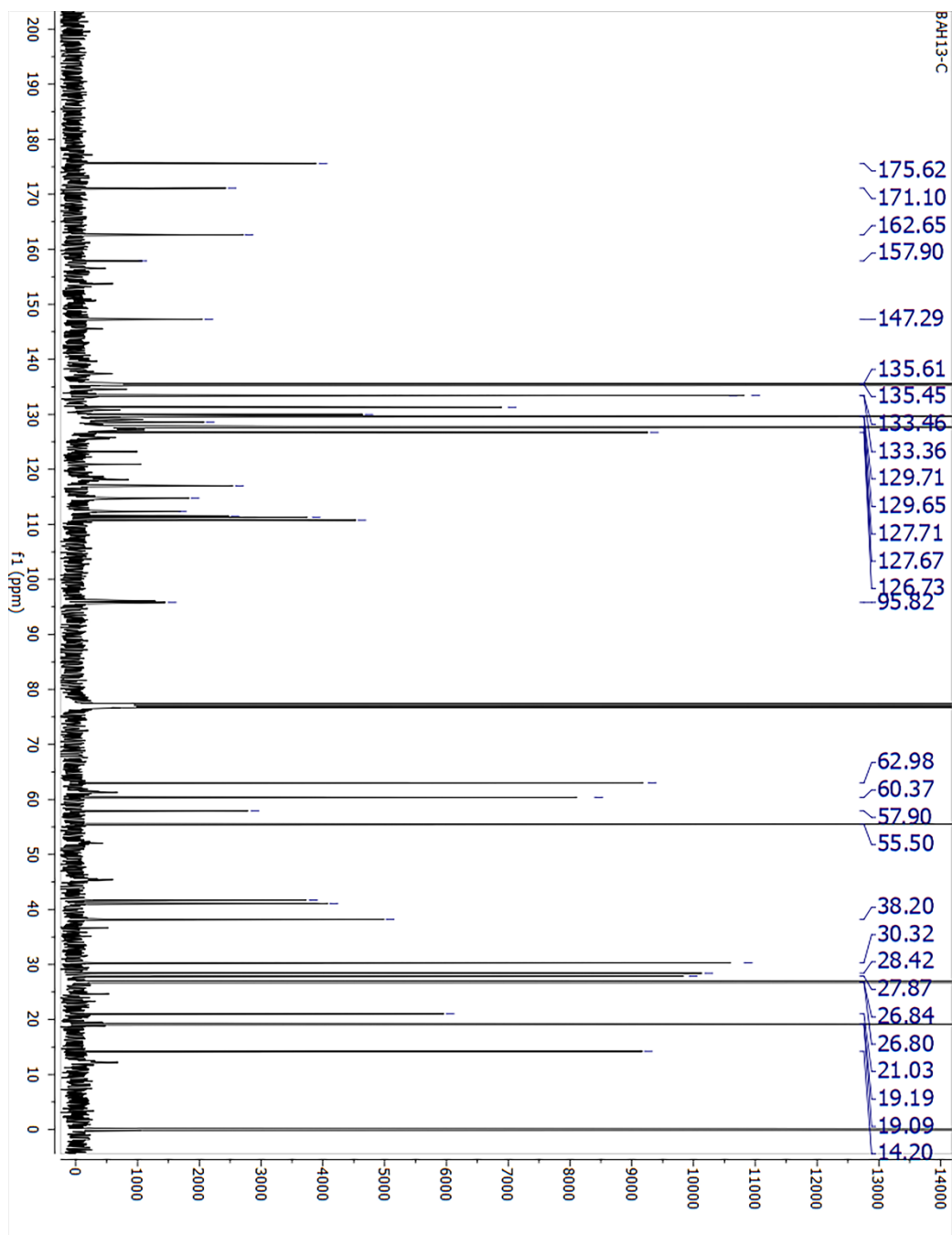


Figure S5. ^{13}C NMR spectrum of BAH13.

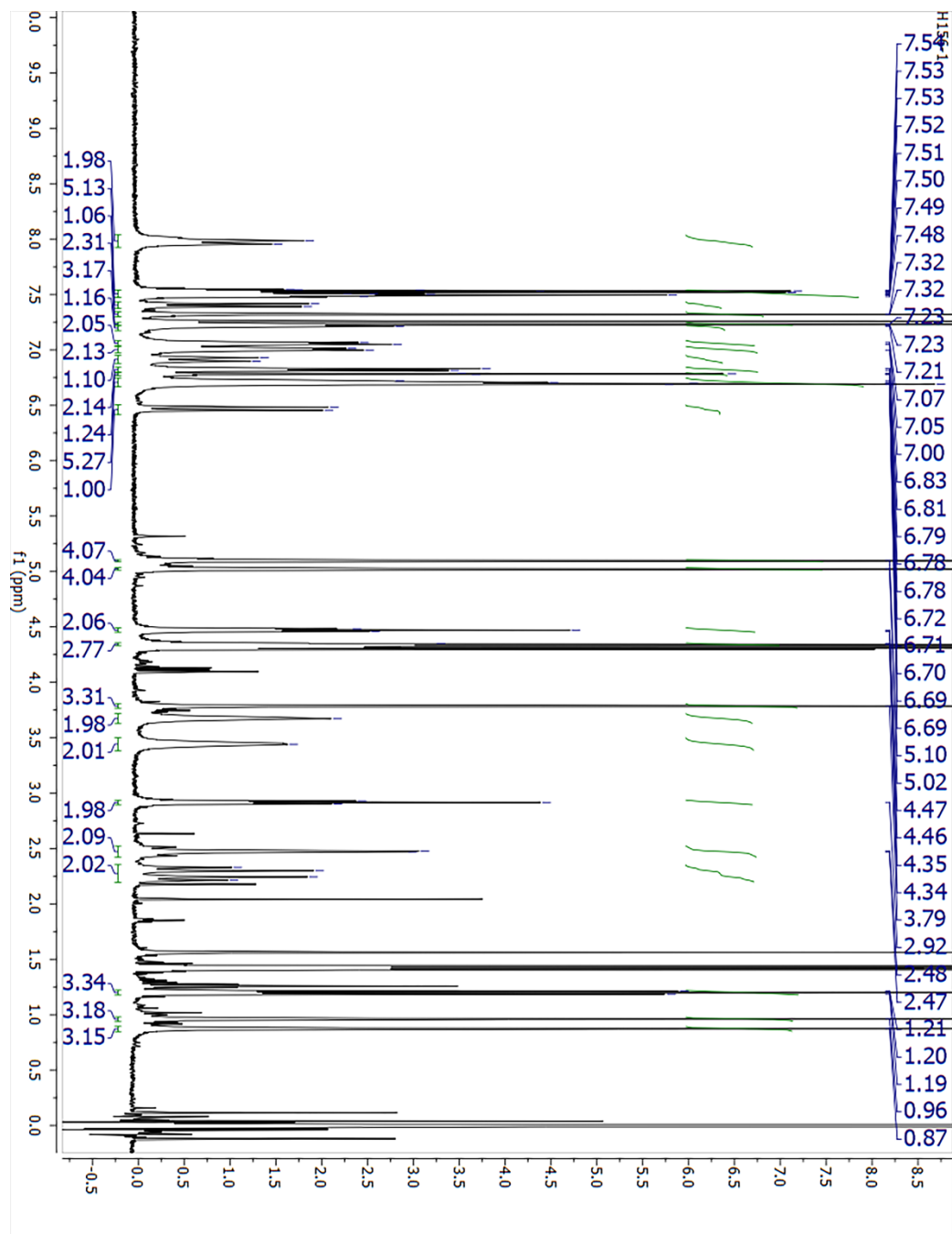


Figure S6. ^1H NMR spectrum of BAH-FD.

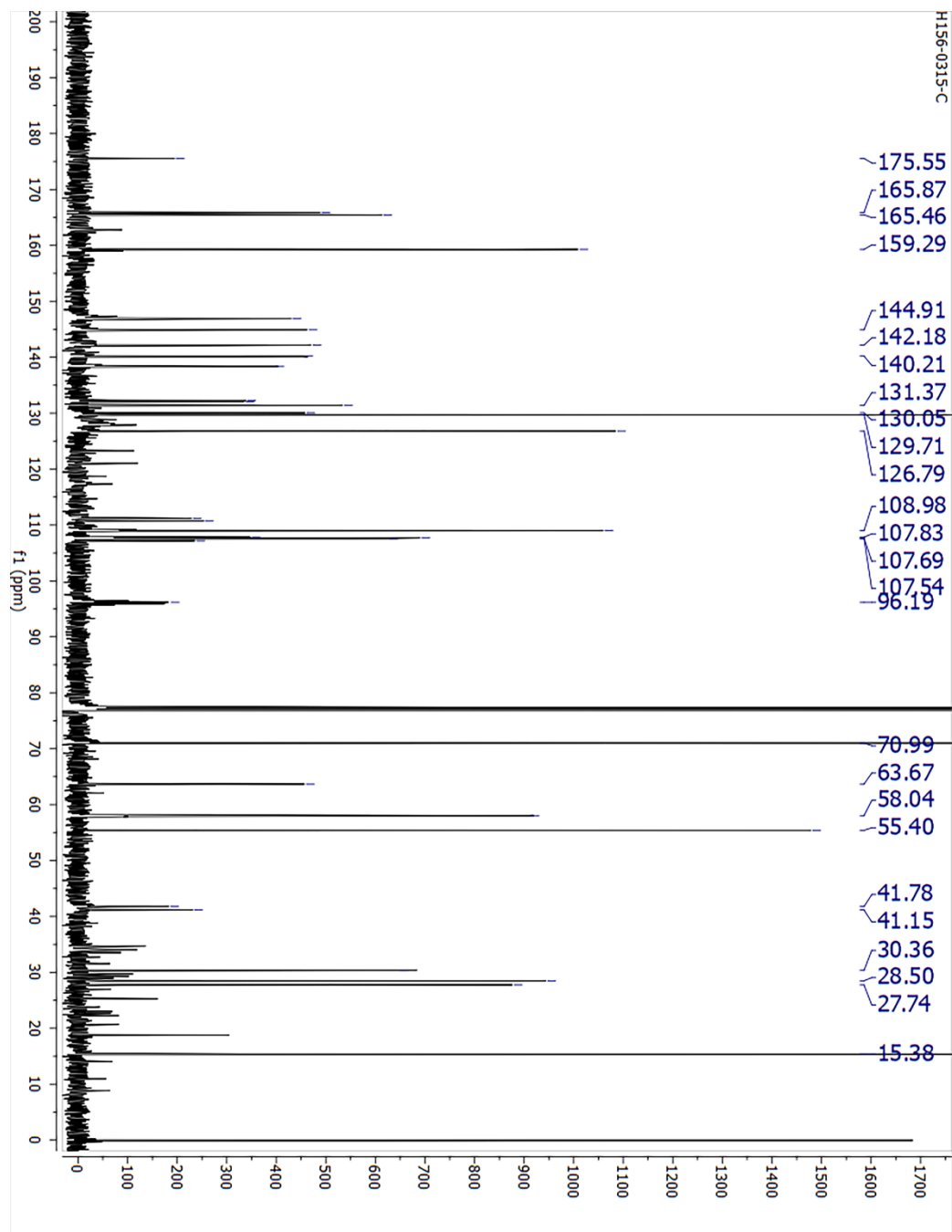


Figure S7. ^{13}C NMR spectrum of BAH-FD.

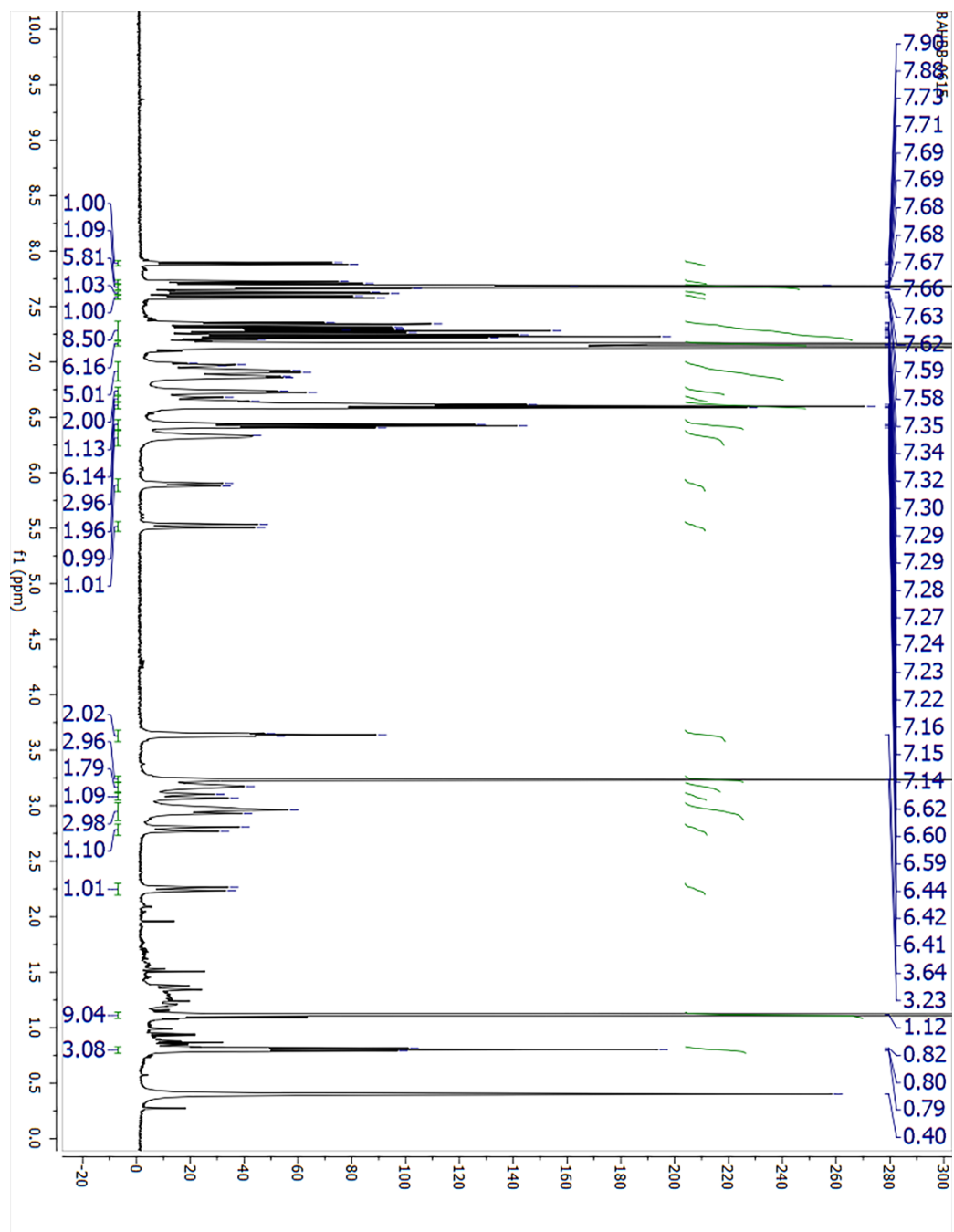


Figure S8. ^1H NMR spectrum of BAH-BB.

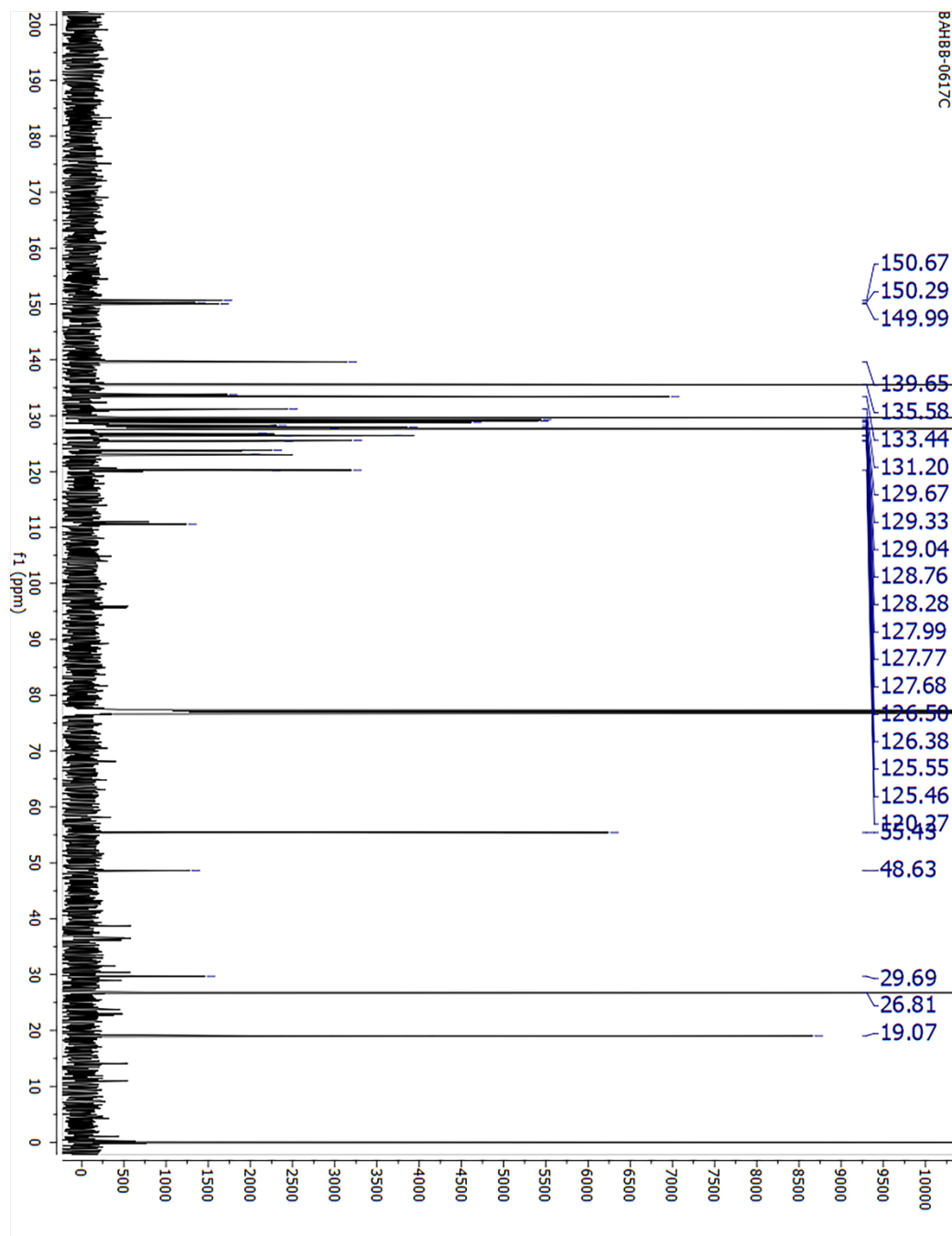


Figure S9. ^{13}C NMR spectrum of BAH-BB.

2. Device Fabrication and Testing.

Device Fabrication Procedure: Solutions of 8-10% w/w EO chromophores in TCE were prepared and sonicated for 5 min to dissolve, filtered through a 0.2 μm PTFE filter, and spin cast onto CBL/ITO substrates. Chromophore in polymer solutions were prepared by combining EO material, poly(methylmethacrylate), and TCE in a vial and sonicated for 20 min to dissolve, filtered through a 0.2 μm PTFE filter, and spin cast onto ITO/glass substrates. EO films were spin cast in three stages, 500 rpm for 5 seconds, 850 rpm for 30 seconds, followed immediately by 1200 rpm for 30 seconds. The films were then dried either in a vacuum oven or at room temperature overnight. The thickness of the EO films were then measured to be around 1-2 μm via optical profilometry. Finally, patterned gold electrodes were deposited on top of the films by sputter coating through a shadow mask, thus completing a device.

Poling procedure: Samples are poled under a constant nitrogen purge in a previously described apparatus that allows for real-time monitoring of current, voltage, temperature, and optical signal correlated r_{33} .² Actual current and voltage drop across the sample are measured (not simply the voltage supplied by the source/measurement unit). First, at room temperature, 5 V/ μm is applied to the device. The sample is then heated on an aluminum block at $\sim 10\text{ }^\circ\text{C min}^{-1}$ to the OEO material T_g (**Table S2**), then the voltage is increased to the desired electric field (in the range of 10 to 100 V/ μm). The device is held at poling temperature for a few minutes ($\sim 3\text{--}5$ min) until molecular orientation is complete, then cooled to room temperature, and then the electric field is removed. After poling and cooling to near room temperature, r_{33} for the poled films were measured using the Teng–Man technique^{3, 4} on a custom apparatus at 1310 nm using the refractive index values measured by VASE. All of our r_{33} measurements are shown in **Figure 5** and **S10**. Standard error in r_{33} and poling efficiency were calculated as in reference.⁵

BAH13 was evaluated in a POH platform which features large bandwidths, small footprint, low power consumption, and can be fabricated on top of CMOS electronics as a post-process. In POH phase modulators, light is coupled from a silicon strip waveguide into a metal–insulator–metal slot waveguide and converted to a surface plasmon polariton (SPP) mode at the gold surface. The SPPs propagate along the gold–dielectric interface. Plasmonics allows light confinement below the diffraction limit as well as enhanced light–matter interaction. The slot waveguide is filled with the OEO material, and the device is poled in a manner similar to bulk devices: the modulator is heated to the T_g then an electric field is applied to the gold waveguide walls that serve as poling electrodes. The Pockels effect of the poled OEO material is used to encode an electrical signal on the phase of the propagating SPPs. At the end of the plasmonic waveguide, the phase modulated SPPs are converted back to photonic modes of the output silicon waveguide by the second taper structure. In this work, the phase plasmonic phase modulators are integrated in an imbalanced silicon–photonic push–pull Mach–Zehnder geometry, Figure 5, in which two phase modulators are oppositely driven. At an applied voltage V_π , each phase modulator produces opposite quarter-wave phase shifts leading to complete destructive interference between the two arms, switching the modulator from the on- to the off-state. The EO performance at 1550 nm is determined in 10- μm long modulators with 80 and 105 nm wide slots operating in the 15 – 70 GHz range. To measure the on-off voltage V_π , the wavelength-dependent intensity transfer function was recorded while applying DC voltages between ± 1 V in steps of 0.5 V.

There are several factors that contribute to the EO performance difference between bulk device Teng–Man measurements at 1310 nm and POH devices at 1550 nm. First, high density OEO materials like 100% BAH13 have a high leakage current at the poling temperature, and charge barrier layers like HfO_2 or TiO_2 are required to sustain a high poling field. Effective barrier layers have not yet been tested with BAH13 in POH devices, and therefore, poling fields were likely less than in the bulk devices. Second, it is known that EO coefficients are lower with narrower slot widths.²⁴ This is due to electrostatic interactions between the organic EO molecules and the slot sidewalls that counteracts the ordering force induced by the poling field. Since the surface region is a larger fraction of the total in narrow slot devices, it is expected that the average acentric order will be lower, and the r_{33} will be lower in 80 and 105 nm slots compared to micron thick films. Despite some r_{33} reduction with slot width, the concentration of light in subwavelength slots and better overlap of optical and electrical fields result in a significantly improved $V_\pi L$ modulator performance metric. Third, β is lower at 1550 nm than at 1310 nm, and r_{33} tracks with this decrease. EO performance at different wavelengths can be estimated from the Two-level Model (TLM) in a manner similar to estimation of frequency dispersion of HRS measurements. The Teng–Man r_{33} measurements were conducted at 1310 nm due to better transparency of ITO and reduced substrate influence on the Teng–Man measurement versus at 1550 nm. For detailed discussion on the influence of operating wavelength and interfacial effects in narrow slots, please see the slot waveguide simulations section in ESI†.

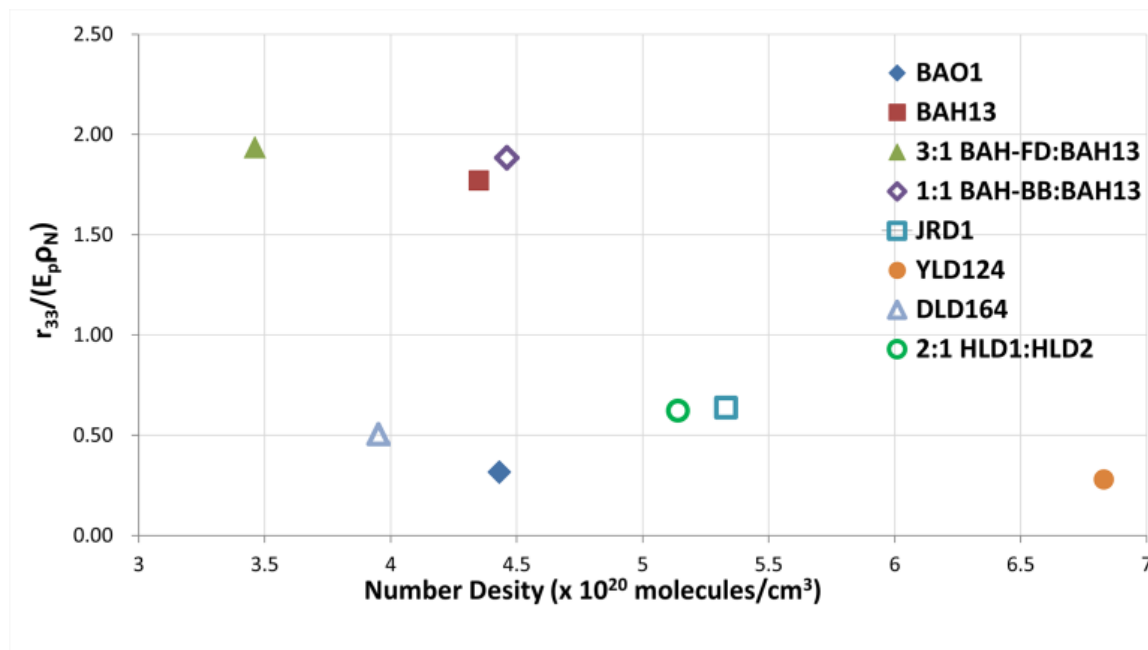


Figure S10. Poling efficiencies per number density of BAH chromophores and the chromophores in literatures.

3. UV-Vis-NIR Absorption Spectra

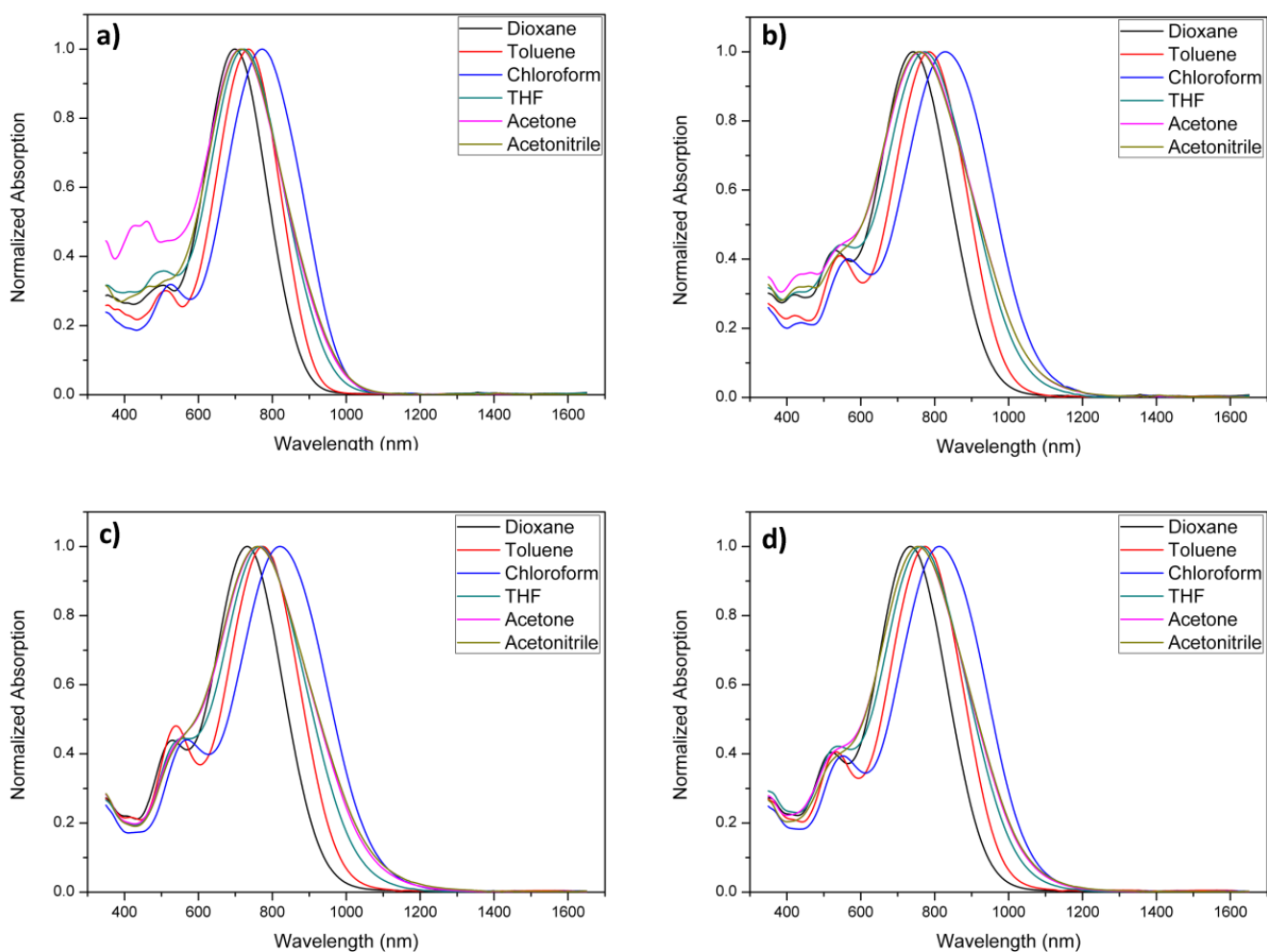


Figure S11. Normalized UV-Vis absorption spectra of chromophores in six aprotic solvents with varying dielectric constants (ϵ). a) BAO1. b) BAH13. c) BAH-BB. d) BAH-FD.

Table S1. UV-Vis λ_{\max} data (nm) of chromophores in various solvents, and as neat thin films

	Dioxane (nm)	Toluene (nm)	Chloroform (nm)	THF (nm)	Acetone (nm)	Acetonitrile (nm)	Film (nm)
BAO1	698	735	772	722	714	715	786
BAH13	742	784	829	772	762	758	850
BAH-BB	731	774	821	768	762	760	835
BAH-FD	735	774	813	762	755	755	820
JRD1	725	751	784	767	777	782	800
BAY1	777	830	890	818	802	800	935

4. Optical constants.

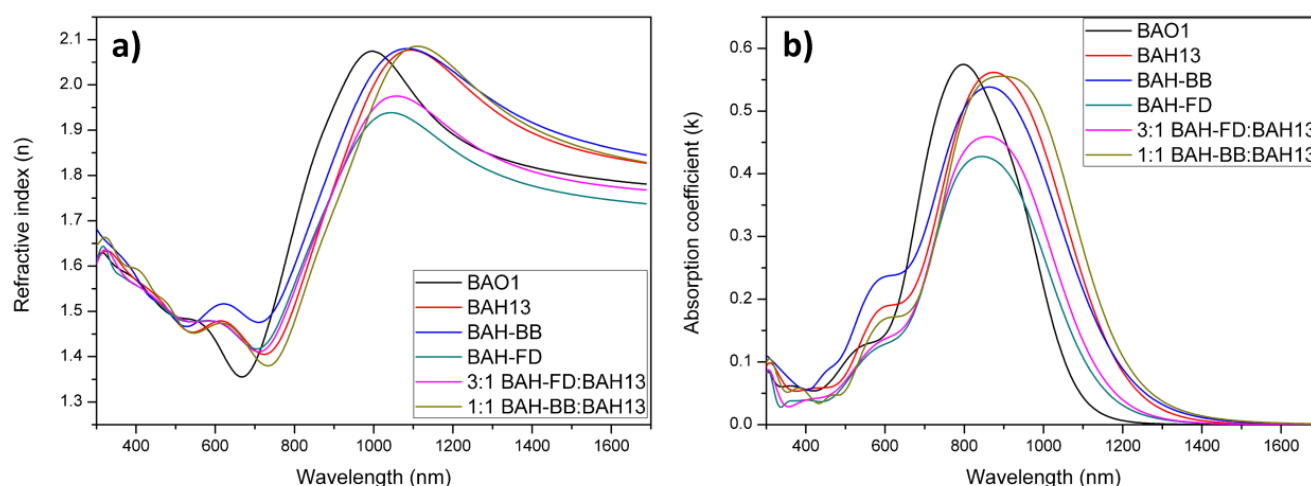


Figure S12. Refractive index (n) and absorption coefficient (k) of films of neat chromophores and their blends.

5. Thermal properties of chromophores

The glass transition temperatures (T_g) and decomposition temperatures (T_d) of the novel chromophores were investigated using thermogravimetric analysis (TGA) and differential scanning calorimetry (DSC) under nitrogen, respectively, and summarized in Table S2. All the chromophores exhibited good thermal stabilities with the T_d s higher than 210 °C (Figure S17), which is typical for isophorone-protected polyene (CLD) chromophores with CF_3Ph -TCF acceptors. All of the chromophores only show T_g in their DSC traces, and no melting points were observed (Figure S13-16), which is desirable as crystallinity can cause scattering or reduce long term device stability. BAH-BB showed a significant enhanced T_g relative to other chromophores presumably because of its rigid bridge structure.⁶

Table S2. Optical constants and thermophysical properties.

Sample	ρ^N ($\times 10^{20}$ molecules/cm ³) ^a	n_{1310}	n_{1550}	k_{1310}	k_{1550}	T_g (°C)	T_d (°C)
100wt% JRD1	5.33	1.91	1.84	0.00010	0.000018	93	226
100% BAY1	4.30	2.02	1.90	0.133	0.0255	84	205
100wt% BAO1	4.43	1.84	1.79	0.00099	0.000042	72	251
100wt% BAH13	4.35	1.94	1.85	0.02126	0.001	78	213
100wt% BAH-BB	4.56	1.96	1.87	0.02906	0.00271	127	261
100wt% BAH-FD	3.17	1.81	1.75	0.00695	0.00041	64	256
1:1 BAH-BB:BAH13	4.46	1.95	1.86	0.03395	0.00381	N/A	N/A
3:1 BAH-FD:BAH13	3.46	1.84	1.78	0.00891	0.000504	N/A	N/A

^a Number density (assumes mass density of 1 g/cm³).

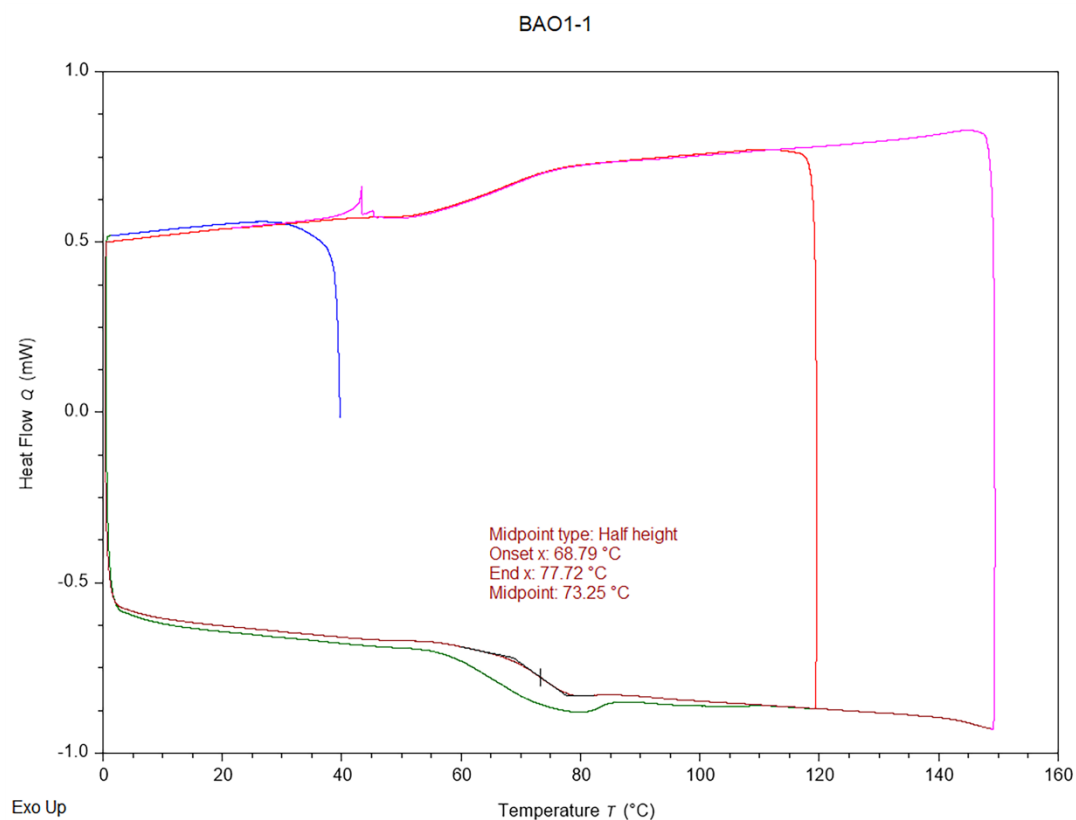


Figure S13. DSC plot of BAO1.

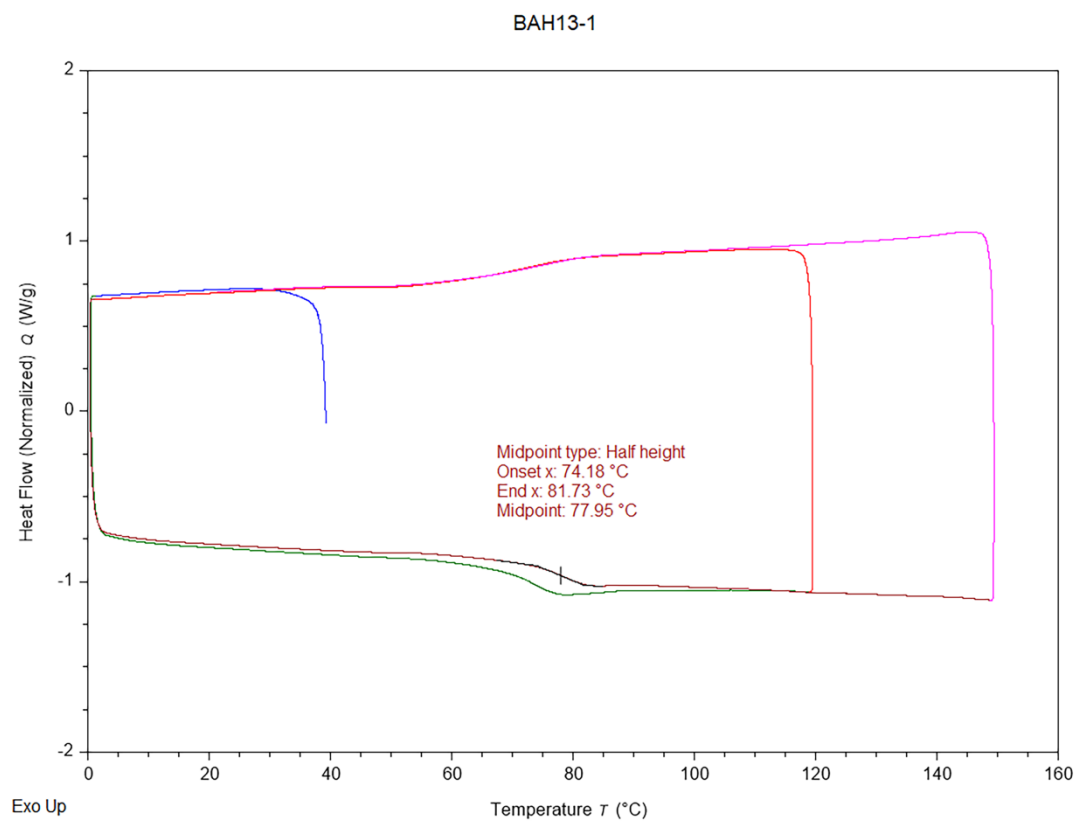


Figure S14. DSC plot of BAH13.

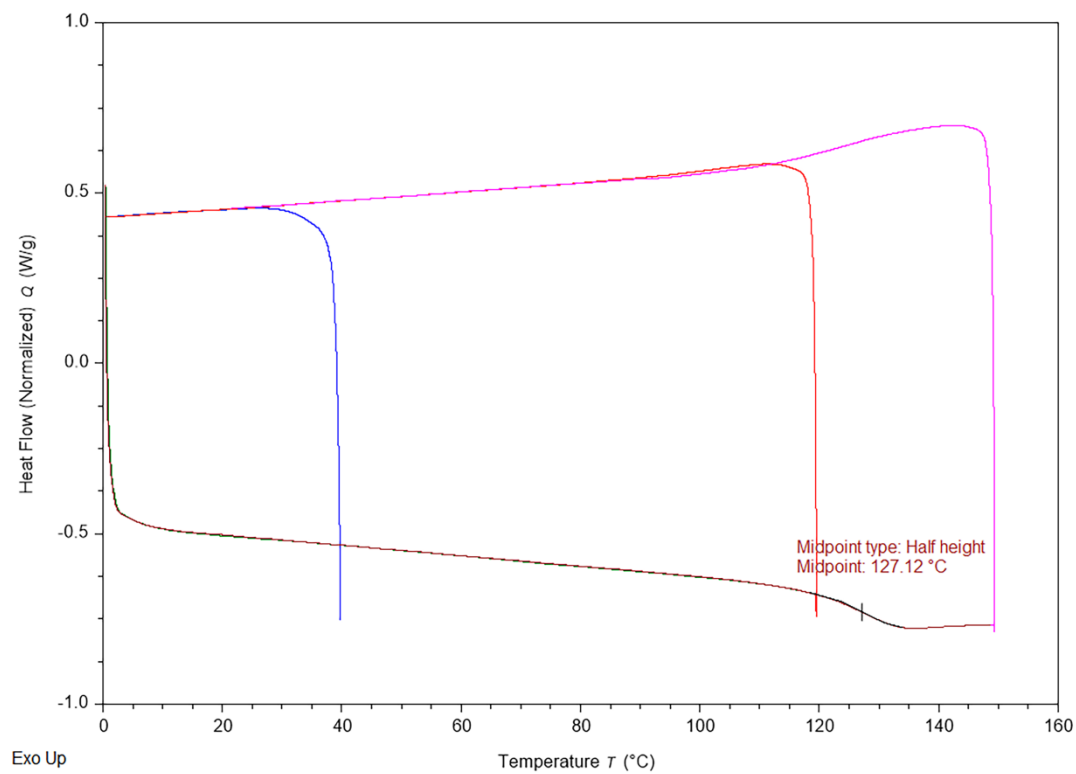


Figure S15. DSC plot of BAH-BB.

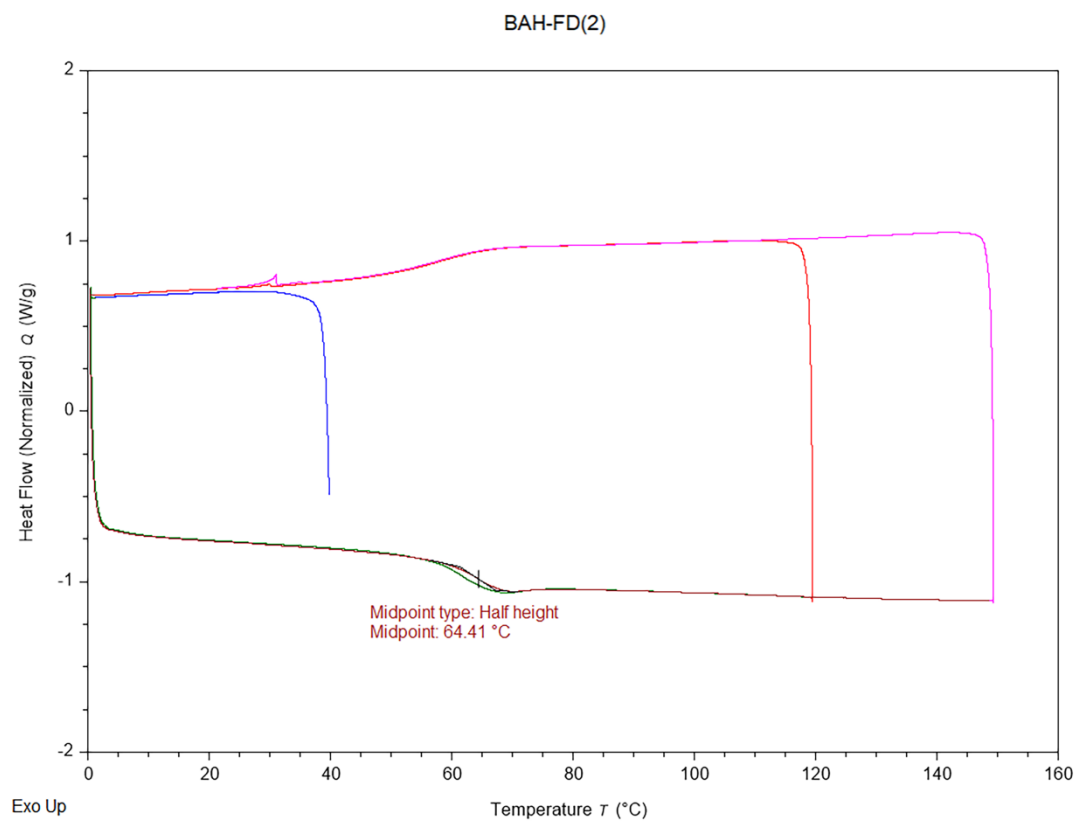


Figure S16. DSC plot of BAH-FD.

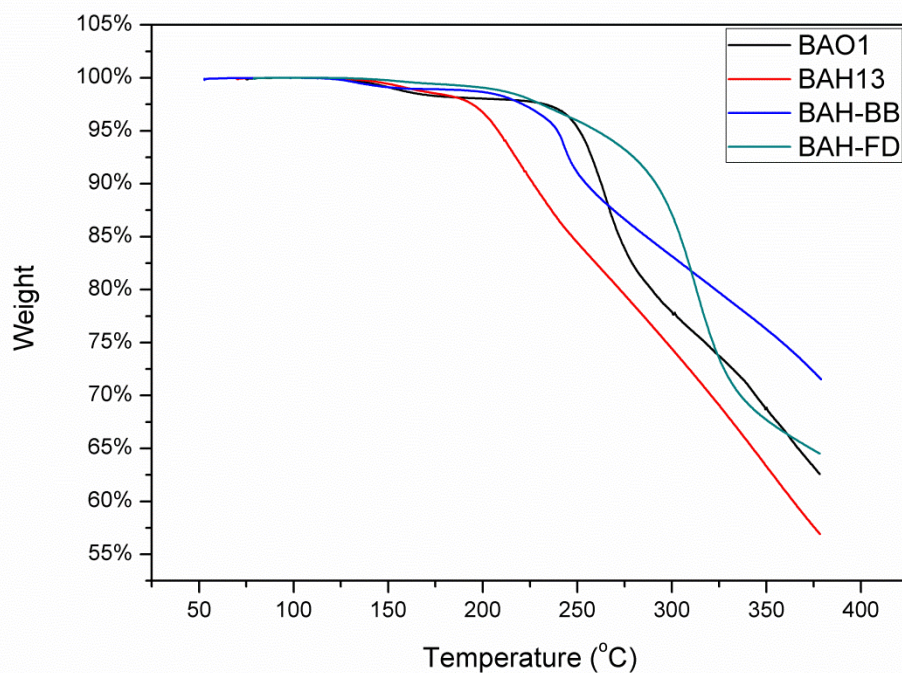


Figure S17. TGA curves of chromophores (powders) with a heating rate of $10\text{ }^{\circ}\text{C min}^{-1}$ in a nitrogen atmosphere.

6. Cyclic Voltammetry

To investigate the electrochemical properties of chromophores under study, cyclic voltammetry (CV) measurements were conducted in degassed anhydrous dichloromethane solutions (**Figure S18**). BAH chromophores exhibited two reversible oxidation waves due to two secondary electron-donating groups. The HOMO and LUMO energy levels were calculated from their corresponding oxidation and reduction potentials, as shown in **Table S3**. Higher HOMO energy levels are expected for stronger electron donor compounds. BAH chromophores have significant higher HOMO energy levels ($-4.70\text{ eV} \sim -4.65\text{ eV}$) than that of JRD1 (-4.96 eV). Conversely, the LUMO energy levels (CV) experienced much smaller variation due to sharing the same acceptor moieties for the novel chromophores and reference molecules. CV optical Band gaps for the BAH chromophores ($0.61 - 0.67\text{ eV}$) were significantly smaller than for JRD1 and BAO1 ($0.93-0.99\text{ eV}$).

Table S3. Electrochemical and optical properties

Sample [*]	$E_{1/2}^{ox2}$ (V)	E_{onset}^{ox2} (V)	$E_{1/2}^{ox1}$ (V)	E_{onset}^{ox1} (V)	E_{peak}^{red} (V)	E_{onset}^{red} (V)	HOMO (eV)	CV LUMO (eV)	CV Band Gap (eV)	Optical Band Gap (eV)	Optical LUMO (eV)
JRD1 ^a			0.455	0.393	-0.680	-0.593	-4.96	-3.98	0.99	1.09	-3.87
BAY1 ^b	0.453	0.402	0.040	-0.033	-0.719	-0.570	-4.53	-4.00	0.54	0.94	-3.59
BAO1			0.470	0.401	-0.620	-0.532	-4.97	-4.04	0.93	1.12	-3.84
BAH13	0.712	0.647	0.1460	0.078	-0.640	-0.552	-4.65	-4.02	0.63	1.01	-3.63
BAH-BB	0.714	0.649	0.150	0.084	-0.608	-0.522	-4.65	-4.05	0.61	1.04	-3.60
BAH-FD	0.744	0.679	0.198	0.129	-0.624	-0.543	-4.70	-4.02	0.67	1.08	-3.62
Ferrocene (sublimed)			0.233								

*Cyclic voltammetry carried out at mM concentrations in dichloromethane solvent with 0.1 M tetrabutylammonium hexafluorophosphate electrolyte. Potentials are relative to 0.01 M Ag/Ag⁺ reference electrode in acetonitrile with 0.1 M tetrabutylammonium hexafluorophosphate electrolyte. $E_{1/2}^{ox}$ is the oxidative half-wave potential. E_{onset}^{ox1} is the onset potential of the first oxidation. E_{onset}^{ox2} is the onset potential of the second oxidation. E_{peak}^{red} is the reductive peak potential (the reduction is not reversible). E_{onset}^{red} is the onset potential of the reduction. HOMO (CV) = -4.8 - (E_{onset}^{ox} [chromophore] - $E_{1/2}$ [ferrocene]) eV. LUMO (CV) = -4.8 - (E_{onset}^{red} [chromophore] - $E_{1/2}$ [ferrocene]) eV. LUMO (optical) = HOMO (CV) + Band gap (optical). Band gap (CV) = LUMO (CV) - HOMO (CV).^a H. Xu, L. E. Johnson, Y. de Coene, D. L. Elder, S. R. Hammond, K. Clays, L. R. Dalton and B. H. Robinson, *J. Mater. Chem. C*, 2021, **9**, 2721-2728. ^b H. Xu, D. L. Elder, L. E. Johnson, Y. de Coene, S. R. Hammond, W. Vander Ghinst, K. Clays, L. R. Dalton and B. H. Robinson, *Adv. Mater.*, 2021, *accepted*, DOI: 10.1002/adma.202104174.

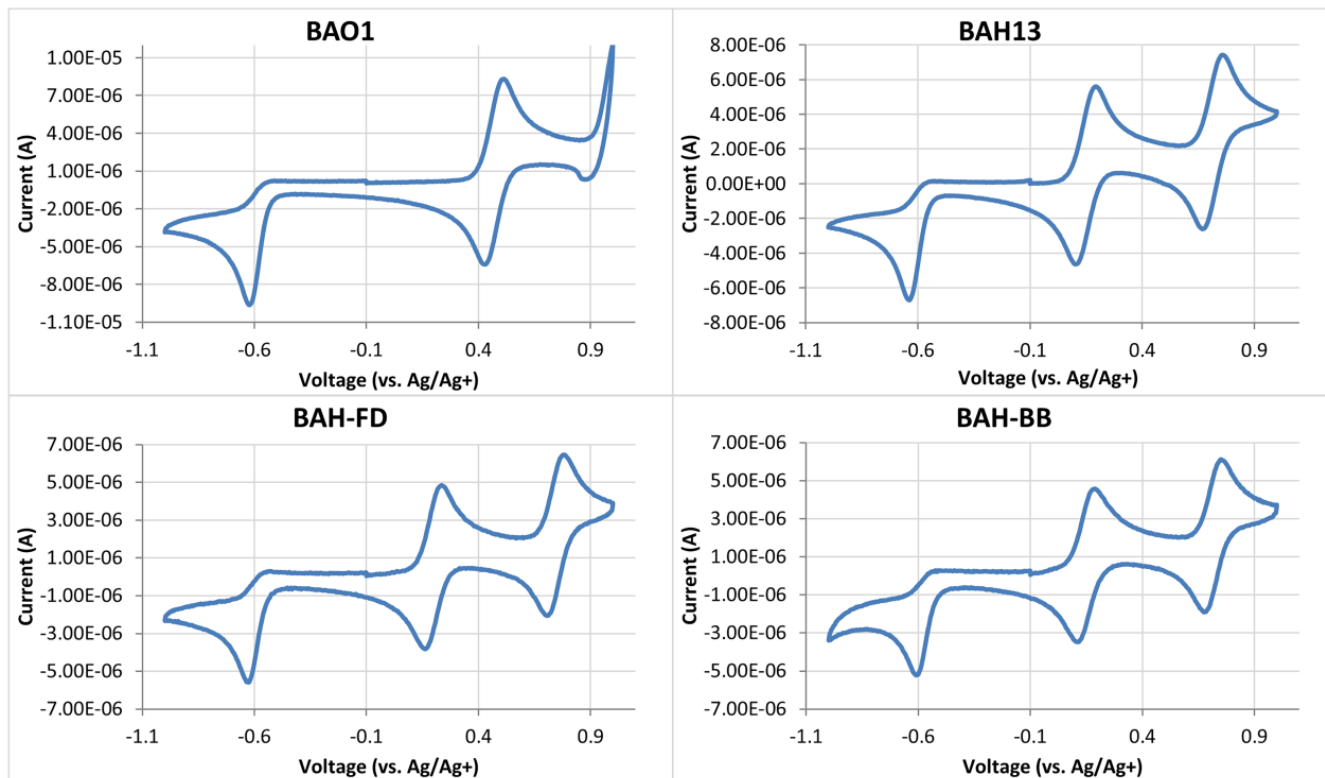


Figure S18. Cyclic voltammogram of chromophores in methylene chloride.

7. Hyper-Rayleigh Scattering

Femtosecond Hyper-Rayleigh scattering⁷ (HRS) measurements were performed in chloroform solution using a custom-built setup at KU Leuven, with detailed methodology reported in literature,⁸ and concurrently with measurements in our recent manuscript on the BTP chromophore family.¹ Measurements were performed using a fundamental wavelength of 1300 nm and a repetition rate of 80 MHz. HRS intensity was corrected for absorption using a Beer-Lambert correction at the second harmonic wavelength. Resonance effects were approximated using the damped two-level model (Equation S1) and a linewidth (γ) of 0.1 eV.⁹ ω_{\max} is the energy corresponding to λ_{\max} .

$$\beta(0) = \frac{\beta(-2\omega; \omega, \omega)}{F(\omega_{laser}, \omega_{\max}, \gamma)}$$

$$F(\omega_{laser}, \omega_{\max}, \gamma) = \frac{\omega_{\max}^2}{3} \left[\frac{1}{(\omega_{\max} + 2\omega_{laser} + i\gamma)(\omega_{\max} + \omega_{laser} + i\gamma)} + \frac{1}{(\omega_{\max} + \omega_{laser} + i\gamma)(\omega_{\max} - \omega_{laser} - i\gamma)} + \frac{1}{(\omega_{\max} - \omega_{laser} + i\gamma)(\omega_{\max} - 2\omega_{laser} + i\gamma)} \right] \quad (S1)$$

The chloroform solvent was used as the reference for the measurements, based on a $\beta_{zz,0}$ value of 0.44×10^{-30} esu⁷ and assuming dipolar symmetry and a single dominant tensor component such that

$$\beta_{zz,0} \approx \sqrt{35/6} \cdot \beta_{HRS,0} \quad (S2)$$

8. DFT Calculations

Closed shell density functional theory (DFT) calculations were performed using Gaussian 09¹⁰ and the M062X functional¹¹ with a 6-31+G(d) basis set in a chloroform implicit solvent environment using default (IEF-PCM) parameters. Structures were optimized in the chloroform environment to RMS force $< 4 \times 10^{-5}$ Hartrees/bohr and maximum force $< 6 \times 10^{-5}$ Hartrees/bohr. Hyperpolarizabilities were calculated via analytic differentiation (CPHF/KS). Calibration of the hyperpolarizability calculation protocol¹² is discussed in Ref. 10. A SCF convergence criterion of $< 10^{-10}$ a.u. RMS in the density matrix was used for all properties calculations. Calculated and experimental (HRS) hyperpolarizability ratios vs. JRD1 are plotted vs differences in first charge transfer band absorption energies vs. JRD1 (ΔE_{\max}) for recent high-performance chromophores (BTP7, BAY1, BAF1, BTF1, BTH1, and BAH13) are plotted in Figure S19, showing how BAH13 was predicted to have improved hyperpolarizability without redshift and how both BAY1 and BAH13 substantially outperformed the experimental and computational trends for the other chromophores.

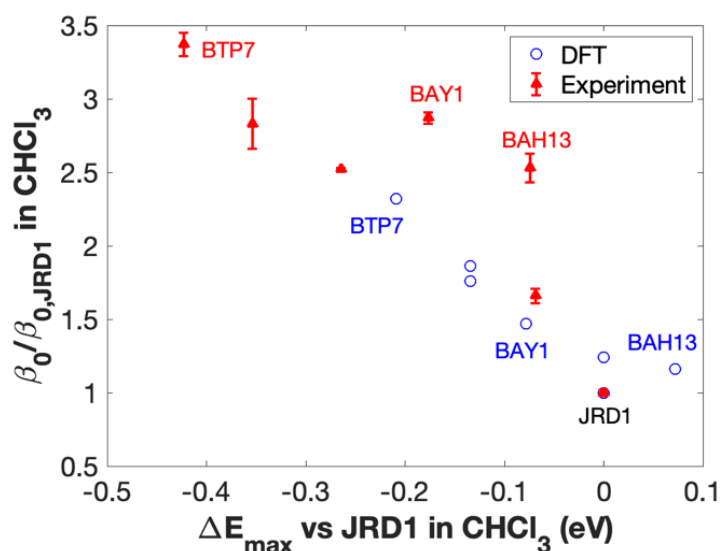


Figure S19. Calculated and experimental hyperpolarizability ratios and shifts in primary charge transfer band for recent high-performance chromophores.

The unusually large performance of the BAH and BAY chromophores relative to their first charge transfer band absorption energy can be analyzed in terms of the two-state model (TSM) for the dominant component of the static hyperpolarizability tensor¹³,

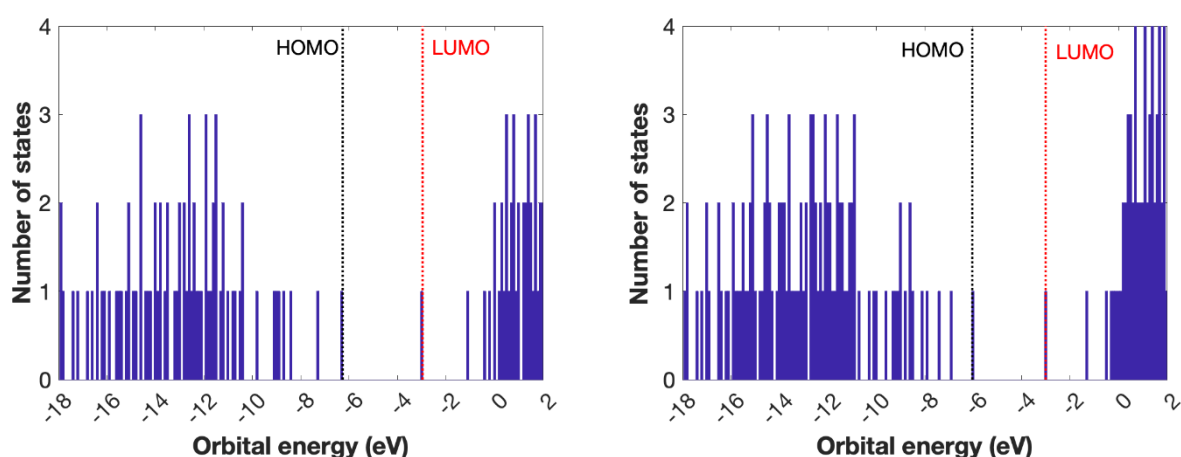
$$\beta_{0,TLM} \propto \frac{\mu_{01}^2 \Delta\mu}{\Delta E_{01}^2} \quad (\text{S3})$$

Which in the convention in which the ground-state dipole μ_0 is defined as parallel to the the z -axis, corresponds to β_{zzz} . Here, μ_1 is the first excited state dipole moment, μ_{01} is the transition dipole between the ground and first excited states, and ΔE_{01} is the energy difference between the ground and first excited state (principal charge transfer excitation energy). DFT-calculated parameters, along with the energy difference between the first and second excited states, are shown in Table S4 for the alkylamine chromophores EZFTC and JRD1 and the arylamine chromophores BTP7, BAY1, and BAH13. Relative TSM hyperpolarizabilities versus JRD1 are reported and compared with the HRS values and CPKS-calculated DFT values in Table 3 and in our recent work on the BTP chromophores¹.

Table S4. Computed key electronic structure descriptors for chromophores

Cpd.	ΔE_{01} (eV)	ΔE_{12} (eV)	μ_0 (D)	μ_1 (D)	$\Delta\mu$ (D)	μ_{01} (D)	$\beta_{rel,TLM}$	$\beta_{rel,CPKS}$	$\beta_{rel,HRS}$
EZFTC	2.16	1.16	25.9	43.7	17.9	16.8	0.65	0.59	0.34 ± 0.09
JRD1	1.88	1.15	31.0	46.1	15.1	19.8	1	1	1 ± 0.02
BTP7	1.69	0.91	34.9	60.7	25.9	21.0	2.40	2.32	3.37 ± 0.08
BAY1	1.83	0.81	30.2	56.4	26.2	19.2	1.73	1.47	2.87 ± 0.04
BAH13	1.89	0.82	28.6	53.4	24.8	19.0	1.49	1.16	2.53 ± 0.10

These data reveal some interesting trends. While BTP7 shows a smaller calculated ΔE_{01} , which clearly contributes to its larger hyperpolarizability, the BAH and BAY chromophores are similar in band gap to JRD1. They do, however, show a much larger first excited state dipole moment μ_1 , which leads to a $\Delta\mu_{01}$ over 60% larger than that of JRD1. Here, the TSM estimate of relative hyperpolarizability is *larger* than the severely underestimated CPKS value. However, the experimentally measured value is still substantially larger than the TSM prediction. This could be explained by an *overestimated* experimental value, e.g. due to the TLM being insufficient to model dispersion,⁹ or the TSM *underestimating* the hyperpolarizability by not fully capturing the electronic structure of the powerful BAX-type donor. Given that the electro-optic data for the BAX chromophores is consistent with the large enhancement in experimental hyperpolarizability, the latter explanation is better supported. The energy difference to the second excited state ΔE_{12} for BTP7 and, in particular, for the BAX chromophores is substantially smaller than for EZFTC or JRD1. To explore this further, we calculated the density of states for JRD1 and BAH13, shown in Figure S20.

**Figure S20.** Density of states for JRD1 (left) and BAH13 (right) calculated at the M062X/6-31+G(d) level of theory in chloroform.

For JRD1, there is a significant gap between the HOMO-1 and lower-lying orbitals, while BAH13 not only has a smaller

HOMO to HOMO-1 gap, but has several higher-energy occupied orbitals. Visualization of the orbitals shows that while both a truncated representation of JRD1 (same truncated representation as the related chromophore YLD124) and BAH13 show significant orbital density near the donor on the HOMO and a significant shift of electron density towards the acceptor in the LUMO (consistent with a large Δu in the TSM), BAH13 has a significant contribution to the HOMO-1 from one of its auxiliary arylamine donors while JRD1 has a relatively symmetric HOMO-1, supporting the hypothesis of contributions from additional orbitals. Orbital isosurfaces are shown in Figure S21.

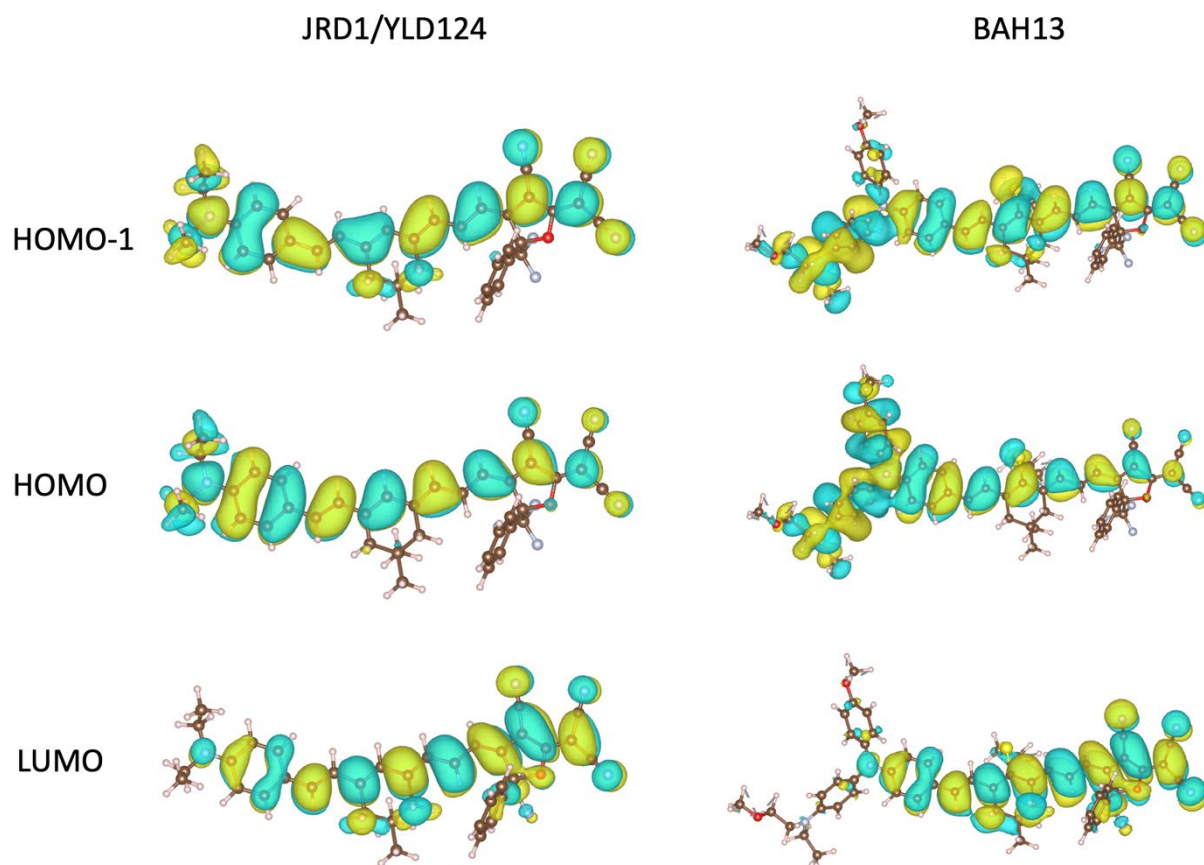


Figure S21. Isosurfaces for HOMO, HOMO-1, and LUMO for truncated models of JRD1 (top row) and BAH13 (bottom row).

9. Slot Waveguide Calculations

POH device performance estimates, including effective index, field confinement, and $V\pi L$, were calculated using Lumerical MODE and the 2D finite difference eigenmode (FDE) solver. Calculations were performed at 1550 nm in a 200 nm high POH metal-insulator-metal (MIM) waveguide on a SiO_2 substrate, varying waveguide width from 30 nm to 150 nm for JRD1 and DLD164 and from 50 nm to 100 nm for BAH13. The optical constants for DLD164 were from our prior work,¹⁴ optical constants for BAH13 were from this work, and newly measured optical constants for commercial material were used for JRD1 ($n_{1550} = 1.84404$, $k_{1550} = 9.0443\text{E-}05$); optical constants of $n_{1550}=0.284$, $k_{1550}=10.22$ were used for gold, and default Palik optical constants for SiO_2 . The MIM waveguide was centered in an 800 nm x 800 nm FDE solver region using the default grid, with a 2.5 nm-spaced mesh override on the slot waveguide with a 10 nm buffer region around it. The dominant TE mode was calculated for each system.

Calculations incorporated an inhomogeneous refractive index and EO coefficient model discussed in our recent

work,¹⁵ which adapts the Singer-Kuzyk-Sohn (SKS)¹⁶ freely rotating dipole model to constrained rotation in response to a poling field (parallel component) and dipole-induced dipole interactions with the metal sidewalls (perpendicular component)

$$\mathbf{f}(x) = \begin{pmatrix} f_{\parallel} \\ f_{\perp}(x) \end{pmatrix} = \begin{pmatrix} \left(\frac{3\epsilon}{2\epsilon + n^2} \right) \frac{\mu E_p}{k_B T} g_k \\ \frac{\rho_N \mu^2}{2k_B T} g_k \cdot \exp\left(-\frac{0.5w - |x|}{\gamma} \right) \end{pmatrix} \quad (\text{S4})$$

and numerically integrating the ordering distribution on a finite set of points along the x axis between $\pm w$, where w is the width of the slot in nm,

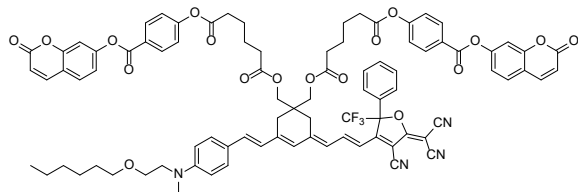
$$\langle \cos^n \theta \rangle_x = \frac{\int_0^{2\pi} \int_0^{\pi} \cos^n \theta e^{f(x) \cos \theta} \sin \theta d\theta d\phi}{\int_0^{2\pi} \int_0^{\pi} e^{f(x) \cos \theta} \sin \theta d\theta d\phi} \quad (\text{S5})$$

Here, μ is the gas-phase dipole moment (~ 25 D for all three chromophores), ϵ is the static dielectric constant, calculated from a scaled Onsager model,¹⁷ n is the isotropic refractive index, T is the poling temperature (in K), ρ_N is the number density of chromophores, g_k is the Kirkwood correlation factor¹⁸⁻²⁰, assumed to be 0.45 for all materials,²⁰ and γ is an empirical decay parameter (8 nm^{-1}) for the interactions with the sidewalls. Parameters for each compound are shown in Table S5.

Table S5. Experimental poling conditions and model parameters

Chromophore	E_p (V/ μm)	T ($^{\circ}\text{C}$)	ρ_N (10^{20} cm^{-3})	f_{\parallel}	$f_{\perp,0}$
DLD164*	100	67	3.95	1.1599	4.7355
JRD1	100	87	5.33	1.1025	6.0349
BAH13	100	87	4.35	1.0959	4.8687

* DLD164 structure:



The refractive index tensor can then be calculated as a function of position based on the degree of poling-induced centrosymmetric order and the isotropic refractive index of the material, using methods discussed in our prior work,^{21,22}

$$\langle P_2 \theta \rangle_x = \frac{3 \langle \cos^2 \theta \rangle_x - 1}{2}$$

$$n_{e,x} = n_{iso} \left(1 + 2s \langle P_2 \theta \rangle_x \right) \quad (\text{S6})$$

$$n_{o,x} = n_{iso} \left(1 - s \langle P_2 \theta \rangle_x \right)$$

The calculated distribution of acentric and centrosymmetric order for BAH13 in a 100 nm slot and resulting refractive index distribution is shown in Figure S22.

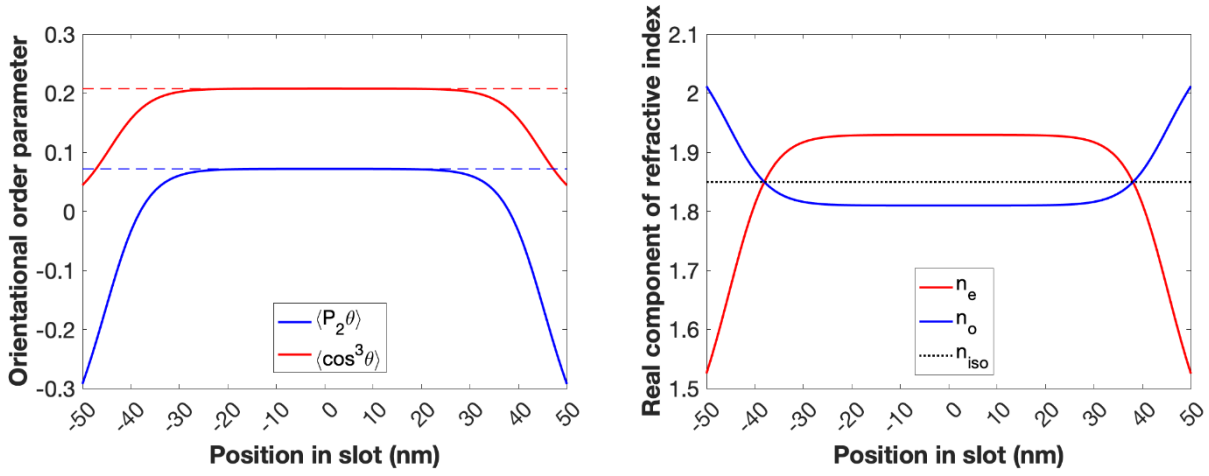


Figure S22. Calculated ordering (left) and index (right) distributions for BAH13 in a 100 nm POH slot

Ordering is reduced near the sidewalls due to electrostatic interactions,²² leading to low- n_e regions near the sidewalls. These index distributions were used to create position-dependent index objects in Lumerical. Results of unperturbed eigenmode calculations in 100 nm wide waveguides are shown in Table S6.

Table S6. FDE calculation results in 100 nm POH waveguides

Material	N_{eff}	Loss α (dB/ μm)	Confinement (% in slot, $\approx 100 \cdot \Gamma$)
DLD164	2.15521+0.0157664i	0.555	65.3133
JRD1	2.15128+0.0134274i	0.473	64.8760
BAH13	2.1738+0.014728i	0.519	65.2751

It can be observed that the mode indices and confinement are very similar for all three materials, and that the predicted optical loss for BAH13 is within 10% of that of JRD1 and below that of DLD164. A position-dependent EO coefficient could be then be calculated in a similar manner, scaling the EO coefficient by the ratio of the local and bulk acentric order,

$$n_e^3 r_{33}(x) = n_{e(x)}^3 r_{33,bulk} \frac{\langle \cos^3 \theta \rangle_x}{\langle \cos^3 \theta \rangle_{bulk}} \quad (\text{S7})$$

Bulk EO coefficients at 1310 nm were specified as 200 pm/V for DLD164, 310 pm/V for JRD1, and 700 pm/V for BAH13 based on prior publications^{14, 23} and this work, which were shifted via the two-level model for the Pockels effect to 1550 nm, yielding 146 pm/V for DLD164, 226 pm/V for JRD1, and 484 pm/V for BAH13. The field distribution and EO coefficient distribution in a 100 nm slot filled with BAH13 are shown in Figure S23. It can be seen that the EO coefficient is highest in the center of the slot and the field is most intense near the gold surface; these effects contribute to the reduction in effective EO coefficient

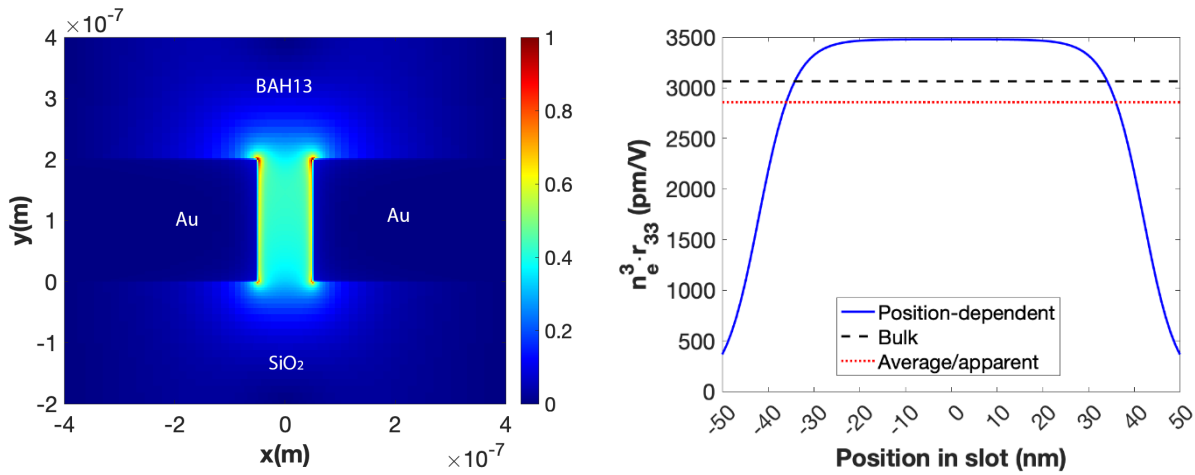


Figure S23. Optical field distribution (right) and EO coefficient distribution (left) in a 100nm slot filled with BAH13

Index perturbations due to the Pockels effect,

$$\Delta n_{e,x} = -\frac{\left(n_e^3 r_{33}\right)_x V}{2w} \quad (\text{S8})$$

were then calculated at $\pm 2V$ based on the EO coefficient and index distributions, and effective indices were calculated at each perturbation. For BAH13 in a 100 nm wide slot, the real component of the index at $-2V$ was 2.15056 and the real component of the index at $+2V$ was 2.1972 for $dN_{\text{eff}}/dV = 0.0117 \text{ V}^{-1}$. The voltage-length project could then be inferred from the transfer function for a balanced MZI at zero bias^{15, 24} as

$$V_\pi L = \frac{\lambda_0}{4} \left| \frac{\partial N_{\text{eff}}}{\partial V} \right|^{-1} \quad (\text{S9})$$

References

1. H. Xu, L. E. Johnson, Y. de Coene, D. L. Elder, S. R. Hammond, K. Clays, L. R. Dalton and B. H. Robinson, *J. Mater. Chem. C*, 2021, **9**, 2721-2728.
2. L. R. Dalton, P. A. Sullivan and D. H. Bale, *Chem Rev*, 2010, **110**, 25-55.
3. C. C. Teng and H. T. Man, *Appl. Phys. Lett.*, 1990, **56**, 1734-1736.
4. Y. Shuto and M. Amano, *J. Appl. Phys.*, 1995, **77**, 4632-4638.
5. W. Jin, P. V. Johnston, D. L. Elder, A. F. Tillack, B. C. Olbricht, J. Song, P. J. Reid, R. Xu, B. H. Robinson and L. R. Dalton, *Appl. Phys. Lett.*, 2014, **104**, 243304-243304-243305.
6. D. L. Elder, C. Haffner, W. Heni, Y. Fedoryshyn, K. E. Garrett, L. E. Johnson, R. A. Campbell, J. D. Avila, B. H. Robinson, J. Leuthold and L. R. Dalton, *Chem. Mater.*, 2017, **29**, 6457-6471.
7. J. Campo, F. Desmet, W. Wenseleers and E. Goovaerts, *Opt Express*, 2009, **17**, 4587-4604.
8. H. J. Xu, F. G. Liu, D. L. Elder, L. E. Johnson, Y. de Coene, K. Clays, B. H. Robinson and L. R. Dalton, *Chem. Mater.*, 2020, **32**, 1408-1421.
9. J. Campo, W. Wenseleers, J. M. Hales, N. S. Makarov and J. W. Perry, *J. Phys. Chem. Lett.*, 2012, **3**, 2248-2252.
10. M. Frisch, G. Trucks, H. B. Schlegel, G. E. Scuseria, M. A. Robb, J. R. Cheeseman, G. Scalmani, V. Barone, B. Mennucci and G. Petersson, *Inc., Wallingford CT*, 2009, **201**.

11. Y. Zhao and D. G. Truhlar, *Theor. Chem. Acc.*, 2008, **120**, 215-241.
12. L. E. Johnson, L. R. Dalton and B. H. Robinson, *Acc. Chem. Res.*, 2014, **47**, 3258-3265.
13. G. Bourhill, J.-L. Bredas, L.-T. Cheng, S. R. Marder, F. Meyers, J. W. Perry and B. G. Tiemann, *J. Am. Chem. Soc.*, 1994, **116**, 2619-2620.
14. D. L. Elder, S. J. Benight, J. S. Song, B. H. Robinson and L. R. Dalton, *Chem. Mater.*, 2014, **26**, 872-874.
15. L. E. Johnson, D. L. Elder, S. J. Benight, A. F. Tillack, S. R. Hammond, L. R. Dalton and B. H. Robinson, presented in part at the SPIE Organic Optics + Photonics, 2021.
16. K. D. Singer, M. G. Kuzyk and J. E. Sohn, *J. Opt. Soc. Am. B*, 1987, **4**, 968-976.
17. L. Onsager, *J. Am. Chem. Soc.*, 1936, **58**, 1486-1493.
18. J. G. Kirkwood, *J. Chem. Phys.*, 1939, **7**, 911-919.
19. L. E. Johnson, R. Barnes, T. W. Draxler, B. E. Eichinger and B. H. Robinson, *J. Phys. Chem. B*, 2010, **114**, 8431-8440.
20. A. F. Tillack, 2015.
21. L. Johnson, D. Elder, A. Kocherzhenko, A. Tillack, C. Isborn, L. Dalton and B. Robinson, presented in part at the SPIE Organic Photonics + Electronics, 2018.
22. B. H. Robinson, L. E. Johnson, D. L. Elder, A. A. Kocherzhenko, C. M. Isborn, C. Haffner, W. Heni, C. Hoessbacher, Y. Fedoryshyn, Y. Salamin, B. Baeuerle, A. Josten, M. Ayata, U. Koch, J. Leuthold and L. R. Dalton, *J. Lightwave Technol.*, 2018, **36**, 5036-5047.
23. W. W. Jin, P. V. Johnston, D. L. Elder, A. F. Tillack, B. C. Olbricht, J. S. Song, P. J. Reid, R. M. Xu, B. H. Robinson and L. R. Dalton, *Appl. Phys. Lett.*, 2014, **104**, 243304.
24. W. Heni, C. Haffner, D. L. Elder, A. F. Tillack, Y. Fedoryshyn, R. Cottier, Y. Salamin, C. Hoessbacher, U. Koch, B. Cheng, B. Robinson, L. R. Dalton and J. Leuthold, *Opt Express*, 2017, **25**, 2627-2653.